Behavioral/Systems/Cognitive

Three Patterns of Oscillatory Activity Differentially Synchronize Developing Neocortical Networks *In Vivo*

Jenq-Wei Yang,* Ileana L. Hanganu-Opatz,* Jyh-Jang Sun, and Heiko J. Luhmann
Institute of Physiology and Pathophysiology, University of Mainz, D-55128 Mainz, Germany

Coordinated patterns of electrical activity are important for the early development of sensory systems. The spatiotemporal dynamics of these early activity patterns and the role of the peripheral sensory input for their generation are essentially unknown. We performed extracellular multielectrode recordings in the somatosensory cortex of postnatal day 0 to 7 rats *in vivo* and observed three distinct patterns of synchronized oscillatory activity. (1) Spontaneous and periphery-driven spindle bursts of 1–2 s in duration and ~10 Hz in frequency occurred approximately every 10 s. (2) Spontaneous and sensory-driven gamma oscillations of 150–300 ms duration and 30–40 Hz in frequency occurred every 10–30 s. (3) Long oscillations appeared only every ~20 min and revealed the largest amplitude (250–750 μV) and longest duration (>40 s). These three distinct patterns of early oscillatory activity differently synchronized the neonatal cortical network. Whereas spindle bursts and gamma oscillations did not propagate and synchronized a local neuronal network of 200–400 μm in diameter, long oscillations propagated with 25–30 μm/s and synchronized 600–800 μm large ensembles. All three activity patterns were triggered by sensory activation. Single electrical stimulation of the whisker pad or tactile whisker activation elicited neocortical spindle bursts and gamma activity. Long oscillations could be only evoked by repetitive sensory stimulation. The neonatal oscillatory patterns *in vivo* depended on NMDA receptor-mediated synaptic transmission and gap junctional coupling. Whereas spindle bursts and gamma oscillations may represent an early functional columnar-like pattern, long oscillations may serve as a propagating activation signal consolidating these immature neuronal networks.

Introduction

Rhythmic network activity can be observed at earliest developmental stages in various neuronal structures, such as the spinal cord (Saint-Amant and Drapeau, 2001; Hanson and Landmesser, 2003), retina (Galli and Maffei, 1988; Meister et al., 1991), and hippocampus (Lahtinen et al., 2002; Leinekugel et al., 2002; Ben-Ari et al., 2007; Crépel et al., 2007). In the immature neocortex, synchronized oscillatory activity may be driven by the periphery (Hanganu et al., 2006; Milh et al., 2007), generated spontaneously by intracortical circuits (Minlebaev et al., 2007; Sun and Luhmann, 2007), or elicited by activation of different metabotropic receptors (Kilb and Luhmann, 2003; Wagner and Luhmann, 2006) (for review, see Khazipov and Luhmann, 2006). Using calcium imaging techniques in the neocortex of newborn rodents *in vitro* and *in vivo*, spontaneous and evoked coordinated activity patterns have been described, which often propagate over large cortical regions (Yuste et al., 1992; Peinado, 2000; Calderon et al., 2005). It has been further demonstrated in the newborn mouse visual cortex that the development of precise cortical maps requires patterned spontaneous activity in the retina (Cang et al., 2005). In the no b-wave (*nob*) mutant mouse, abnormally patterned retinal activity causes a failure in the refinement of the retinogeniculate circuitry (Demas et al., 2006). Correlated rhythmic activity seems to be critical for the establishment of proper connectivity and cortical maps already during an early developmental phase, the so-called precritical period (Feller and Scanziani, 2005). During this period, normal activity patterns are also required for the expression of specific guidance molecules (Nicol et al., 2007). However, the exact nature of the *in vivo* activity patterns and their spatial and temporal properties are still not elucidated.

Here we studied with multielectrode recording techniques the normal activity patterns in the rat primary somatosensory cortex (S1) during the first postnatal week *in vivo*. In contrast to calcium imaging techniques, electrophysiological recordings offer the advantage that the properties of the neuronal activity, e.g., frequency, synchronization, and coherence of oscillations, can be characterized in more detail. The *in vivo* approach offers also the advantage that the afferent and intracortical circuitry is intact and that the role of the sensory input in triggering neocortical activity can be studied under physiological conditions. Here we report that three patterns of oscillatory activity with distinct properties and spatiotemporal organization can be observed in the newborn rat somatosensory cortex *in vivo*. These coordinated patterns may contribute to the establishment of early cortical networks.

Received Nov. 26, 2008; revised May 29, 2009; accepted June 7, 2009.

This work was supported by the Deutsche Forschungsgemeinschaft. J.-W.Y. and J.-J.S. are members of the neuroscience graduate school at the University of Mainz (Deutsche Forschungsgemeinschaft GRK 1044). We thank Drs. J. Staiger, C. Petersen, W. Kilb, A. Borgdorff, and D. Lapray for helpful suggestions and B. Krumm for excellent technical assistance.

*J.-W.Y. and I.L.H.-O. contributed equally to this work.

Correspondence should be addressed to Heiko J. Luhmann, Institute of Physiology and Pathophysiology, University of Mainz, Duesbergweg 6, D-55128 Mainz, Germany. E-mail: luhmann@uni-mainz.de.

I. L. Hanganu-Opatz's present address: Center for Molecular Neurobiology, University Medical Center Hamburg-Eppendorf, Martinistrasse 52, 20251 Hamburg, Germany.

DOI:10.1523/JNEUROSCI.5646-08.2009

 0270-6474/09/299011-15$15.00/0

Materials and Methods

Surgical preparation. All experiments were conducted in accordance with the national laws and the National Institutes of Health guidelines for the use of animals in research and approved by the local ethical committee. Extracellular recordings were performed in S1 (0–3 mm posterior to bregma and 1–4.5 mm from the midline) of postnatal day 0 (P0) to P7 rats (Paxinos et al., 1991) using experimental protocols as described previously (Hanganu et al., 2006, 2007). Briefly, under deep ice-cooling anesthesia alone or combined with light intraperitoneal urethane injection (0.5–1 g/kg; Sigma-Aldrich), the head was fixed into the stereotaxic apparatus using two metal bars fixed with dental cement on the nasal and occipital bones, respectively. The bone, but not the dura mater, over S1 was carefully removed by drilling a hole of <1 mm in diameter. Afterward, the body of the animals was surrounded by cotton and kept at a constant temperature of 37°C by placing it on a heating blanket. During recordings, urethane anesthesia (0.1–0.5 times the original dose) was given when the pups showed any sign of distress. After 30–60 min recovery, multielectrode arrays were inserted perpendicularly into S1 to obtain simultaneous recordings of field potential (FP) and multiple-unit activity (MUA) at different depths and locations. The electrodes were labeled with 1,1′-dioctadecyl-3,3,3′,3′-tetramethyl indocarbocyanine (DiI) (Invitrogen) to enable postmortem in histological sections the reconstruction of the electrode tracks in S1 (see Figs. 1*A*, 4*Bi*). One silver wire was inserted into the cerebellum and served as ground electrode.

Recording and stimulation protocols. FP and MUA recordings were performed using a one-shank or a four-shank 16-channel Michigan electrode (1–2 MΩ; NeuroNexus Technologies) inserted in dorsoventral direction in one hemisphere or in both hemispheres at homologous stereotaxic coordinates. The recording sites were separated by 200 μm in vertical and horizontal direction for the four-shank electrode (Fig. 1*Ai*) and by 50 μm in vertical direction for the one-shank electrode. Both FP and MUA were recorded for at least 1000 s at a sampling rate of 1, 5, or 20 kHz using a multi-channel extracellular amplifier and the MC_RACK software (Multi Channel Systems). Tactile stimulation of all whiskers at a frequency of ~1 Hz was performed by hand. Extracellular direct current (DC) recordings were obtained by using an InstruTECH LIH 8 + 8 data acquisition system (HEKA) at a sampling rate of 5 kHz with a glass pipette filled with artificial CSF (ACSF). The data were digitized online with TIDA software program (HEKA). A spreading depression was elicited by local microdrop (~100 nl) application of 1 M KCl on the neocortical surface near the recording site via a broken glass pipette.

For electrical stimulation of the whisker pad, electrical pulses (40 V, 100 μs) were applied via a bipolar tungsten electrode (160 μm diameter; California Fine Wire Company) inserted 1.5–2 mm through the skin into the whisker pad. Low-frequency stimulation at 0.1 Hz was used to prevent accommodation.

Pharmacological procedures. Neuropharmacological experiments were performed by the use of a 26 gauge needle (World Precision Instruments) attached to a microsyringe pump controller (Micro4; World Precision Instruments). The needle was positioned on the cortical surface close to the one-shank 16-channel Michigan electrode, and 200 nl of the drug was applied at a rate of 50 nl/min. The following substances were applied: DL-APV (100 μM) from Tocris Bioscience, carbenoxolone (100 μM), and lidocaine hydrochloride monohydrate (2%) from Sigma-Aldrich. All solutions were prepared on the day of the experiment in ACSF containing the following (in mM): 124 NaCl, 26 $NaHCO_3$, 1.25 NaH_2PO_4, 1.8 $MgCl_2$, 1.6 $CaCl_2$, 3 KCl, and 10 glucose, pH 7.4. Control experiments with application of ACSF without drug were performed before APV or carbenoxolone application. Lidocaine application was performed to certify the diffusion ability of applied solutions into the neocortex at the recording site.

Blockade of neuronal activity from the whiskers to S1 via the trigeminal nerve was achieved by injection of 20 μl of lidocaine (2% in saline) subcutaneously into the face just adjacent to the whisker pad.

Data analysis. Data were imported and analyzed offline using MATLAB software versions 6.5 and 7.7 (MathWorks). To detect the oscillatory events, the raw data were filtered between 5 and 80 Hz using a Butterworth three-order filter. Oscillatory events were detected as FP deflections exceeding five times the baseline SD. Only events lasting >100 ms and containing more than three cycles were considered for analysis. The events were analyzed in their occurrence, duration, amplitude (voltage difference between the maximal positive and negative peak), maximal frequency within each event, and relative frequency fraction corresponding to the theta (4–8 Hz), alpha (8–13 Hz), and beta (13–30 Hz) frequency bands. Time–frequency plots were calculated by transforming the FP events using Morlet continuous wavelet (Sun and Luhmann, 2007). Minimal and maximal intensities in power were normalized to values between 0 and 1 and were displayed in dark blue and red, respectively. Correlation between oscillatory events recorded at different sites was assessed by cross-correlation and coherence analysis. The maximal cross-correlation and coherence coefficients were calculated by selecting one channel as reference. As spectral measure of correlation between two signals across frequencies, the coherence was calculated from the cross-spectral density between the two signals and normalized by the power spectral density of each (Jerbi et al., 2007). The computation was performed according to the following formula:

$$C(f) = \frac{\left| \sum_{i=1}^{N} X_i(f) Y_i^*(f) \right|^2}{\sum_{i=1}^{N} |X_i(f)|^2 \sum_{i=1}^{N} |Y_i(f)|^2},$$

where $X_i(f)$ and $Y_i(f)$ are the Fourier transforms of the signals x and y for the i data segment at frequency f, and * indicates the complex conjugate. The computations were performed by using the magnitude-squared coherence function (MATLAB) based on Welch's averaged periodogram method (nonoverlapping 0.5 s time window, frequency resolution of 2 Hz). Coherence values ranging from 0 (events are uncorrelated) to 1 (events are perfectly correlated) were encoded from dark blue (0) to red (1) and displayed in coherence maps for all 16 recorded channels. After 200 Hz high-pass filtering, MUA was detected by the threshold of fivefold baseline SD. To measure the phase synchronization between the local FP and MUA, a modified cross-correlation quantification was used (Lu et al., 2005). MUA discharge was detected when the positive value was higher than sevenfold baseline SD. The peaks of the negative trough of the field potential oscillations were used as reference to calculate the cross-correlation histograms with a 2 ms bin width. The values of cross-correlation histograms ranged between 0 (no synchronization) and 1 (perfect synchronization). Current source density analysis (CSD) profiles were calculated from the field potential profiles according to a five-point formula described by Nicholson and Freeman (1975). The CSD values I_m were derived from the second spatial deviation of the extracellular field potentials Φ and calculated by the following finite-difference formula:

$$I_m = -(1/kh^2) \sum_{m=-n}^{n} a_m \Phi(X + mh),$$

where h is the distance between successive measuring points (50 μm in the present investigation), and X is the coordinate perpendicular to the cortical layer. The remaining constants are as follows: $n = 2$, $k = 4$, $a_0 = -2$, $a_{\pm 1} = 0$, and $a_{\pm 2} = 1$. In the CSD profiles, current sinks are indicated by downward deflections and sources by upward deflections. To facilitate visualization of CSD profiles, we generated color image plots by linear interpolation along the depth axis. The blue color represented current sinks, and red color represented current sources.

The stereotaxic coordinates of the barrel cortex were obtained for each pup by scaling the previously reported stereotaxic coordinates of the adult barrel cortex (Welker, 1976; Paxinos et al., 1991) to the age-dependent changes along the bregma–lambda distance. In 24 pups, the resulting coordinates were confirmed by tactile or electrical stimulation of the whiskers. In the graphical reconstructions of the barrel field (see Figs. 3, 5, 7, light blue landmarks), age-dependent topographic changes within S1 were taken into account, and the calculated stereotaxic coordinates were normalized to the lateral and posterior borders (100%) of the barrel field. To estimate any relationship between the properties of oscillatory activity and the stereotaxic location in S1, the occurrence, amplitude, duration, and frequency of oscillations were averaged, nor-

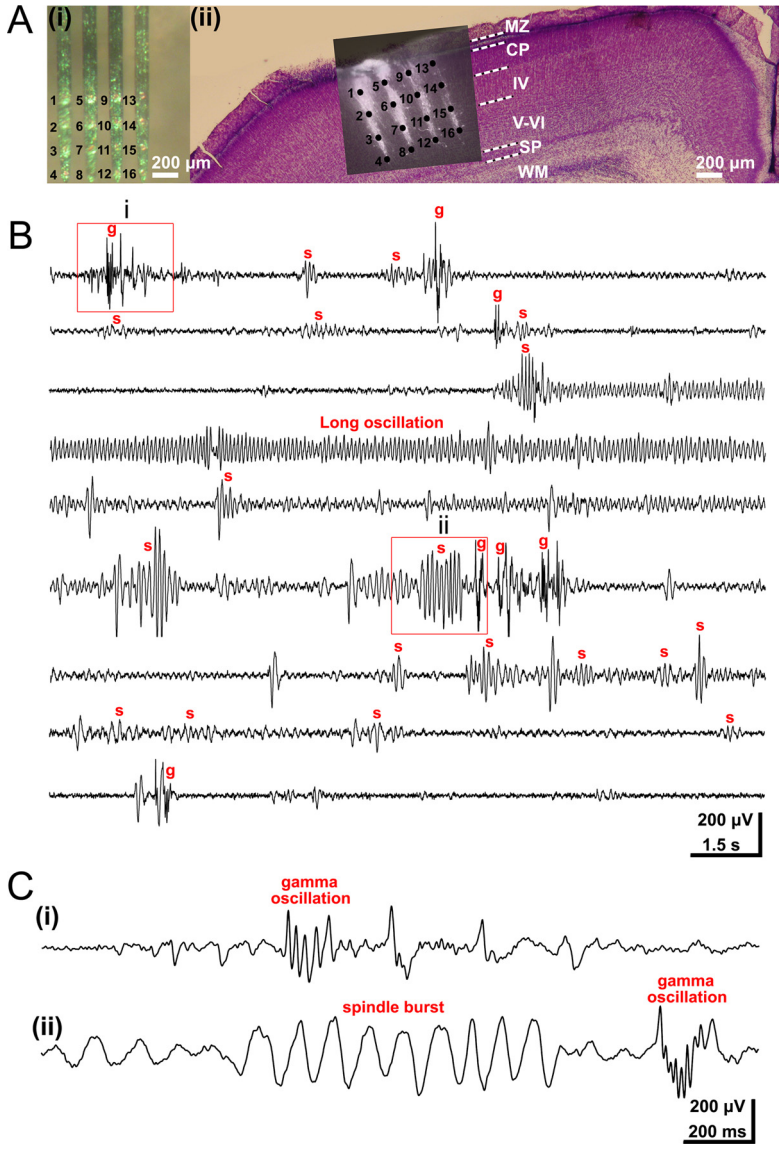

Figure 1. Three distinct patterns of oscillatory activity in the S1 of the neonatal rat *in vivo*. ***A***, Multielectrode array used for extracellular recording of the S1 network activity at different cortical depths and locations. ***i***, Photograph of the 4 × 4-channel Michigan electrode array covered with DiI crystals. The 16 recording sites are marked by numbers. ***ii***, Digital photomontage reconstructing the location of the DiI-covered electrode array in S1 of a Nissl-stained 200-μm-thick coronal section from a P3 rat. Black dots and black numbers correspond to those in ***i*** and mark the 16 recoding sites in different cortical layers. ***B***, Continuous recording of spontaneous activity at electrode 9 from ***Aii***. Several spindle bursts (marked by s), gamma oscillations (g), and one long oscillation could be recorded during this 135-s-long observation period. Note the similar properties of spindle bursts and gamma oscillations before and after the long oscillation. ***C***, Examples of gamma oscillations (***i***, ***ii***) and spindle burst (***ii***) displayed at expanded timescale and marked in by red boxes in ***B***.

malized to the maximal value from each animal, and displayed in color codes: red dots for normalized values exceeding 50% of the maximal values, yellow dots for normalized values ranging between 25% and 50% of the maximal values, and black dots for normalized values below 25% of the maximal value (see Figs. 3*A*, 5*A*, 7*A*).

Cluster analyses of the field potential oscillatory events were performed by the use of the *k*-means algorithm in MATLAB 7.7. The Silhouette validation method was used to calculate and identify the best clustering (number of cluster) (Rousseeuw, 1987).

Data in the text are presented as mean ± SD. In the bar diagrams, data are shown as box plots giving the median, 25th and 75th percentiles, whiskers (10th and 90th percentiles), and outliers using SigmaPlot2001 software (SPSS). Statistical analyses were performed with Systat (SPSS) using Student's *t* test and Mann–Whitney–Wilcoxon test. The significance levels of cross-correlation and coherence values (see Figs. 4*Aii*, 6*Aii*, 8*Aii*, 9*B*) were determined by the use of the *Z*-test (Sun and Luhmann, 2007).

Results

Neonatal somatosensory cortex expresses three distinct patterns of spontaneous oscillatory activity

We examined the activity patterns in the S1 by performing long-lasting extracellular recordings of the local FP in neonatal (P0–P7) rats ($n = 50$ pups) *in vivo* (Fig. 1*A*). Three distinct patterns of spontaneous oscillatory activity could be reliably observed in neonatal S1 (Fig. 1*B*, *C*) (supplemental Movie 1, Fig. 1, available at www.jneurosci.org as supplemental material). As reported previously (Khazipov et al., 2004; Hanganu et al., 2006), the dominant activity pattern recorded in all investigated pups ($n = 50$) was an intermittent network burst associated with spindle-shaped field oscillation that was defined as a spindle burst (Figs. 1*B*, *Cii*, 2*A*). These FP oscillations with a relative short duration (1.4 ± 1.6 s; $n = 918$ events from 50 pups) had an average maximal amplitude of 262.4 ± 317.5 μV ($n = 918$) and occurred at a frequency of 5.3 ± 3.4 bursts/min ($n = 50$ pups). The dominant frequency within a spindle burst ranged in the alpha band with an average maximal frequency of 9.3 ± 4.4 Hz ($n = 918$). However, a certain amount of theta (40.1 ± 21.9% of relative power; $n = 918$) and beta (27.6 ± 20.1% of relative power; $n = 918$) band activity also contributed to the spindle burst pattern. The spindle bursts were associated with rhythmic multiple unit discharges (Fig. 2*A*, MUA trace). To estimate the degree of synchronization between the spindle bursts and MUA, we calculated the cross-correlation by correlating the negative peak of each oscillatory cycle with the spike discharge (supplemental Fig. 2*A*, available at www.jneurosci.org as supplemental material). The resulting high cross-correlation of 0.48 ± 0.22 ($n = 10$ pups) indicates a synchronization of spike discharges with the network oscillations and demonstrates the contribution of single-cell firing to the generation of spindle bursts (supplemental Fig. 2*D*, available at www.jneurosci.org as supplemental material).

Although previous studies defined the spindle burst as the dominant activity pattern in the neonatal somatosensory and visual cortex (Khazipov et al., 2004; Hanganu et al., 2006), we identified two additional patterns of spontaneous oscillatory activity, which so far have not been described *in vivo* (for gamma activity in newborn rat hippocampus *in vitro*, see Palva et al., 2000). In 64% of the investigated pups ($n = 32$), fast oscillations with an average frequency of 38.3 ± 7.7 Hz could be recorded ($n = 495$ events from 32 pups) (Figs. 1*B*, *Ci*, 2*B*). We defined this activity pattern as gamma oscillation, because the dominant frequency of this intermittent and short oscillatory event was in the

gamma frequency range (Palva et al., 2000). Although the occurrence of gamma oscillations (5.8 ± 3.8 events/min; $n = 32$ pups) was similar to that of spindle bursts, their duration was significantly ($p < 0.001$) shorter (0.2 ± 0.2 s; $n = 495$ events from 32 pups) and their amplitude significantly ($p < 0.001$) smaller (138.6 ± 131.2 μV; $n = 495$) than those of spindle bursts. The different frequency distribution, duration, and spatiotemporal properties reinforced the conclusion that spindle bursts and gamma oscillations are two distinct patterns of neuronal activity (supplemental Fig. 1, available at www.jneurosci.org as supplemental material). Gamma oscillations were highly correlated with MUA (average cross-correlation of 0.77 ± 0.17; $n = 10$ pups) (supplemental Fig. 2*B*, *D*, available at www.jneurosci.org as supplemental material).

Beside spindle bursts and gamma oscillations, a third spontaneous activity pattern could be recorded in 20 of 50 investigated pups (Figs. 1*B*, 2*C*). These oscillations were surprisingly long (21–113 s; mean, 54.5 ± 20.2 s; $n = 51$ events from 20 pups) and therefore were termed long oscillations. Despite their rare occurrence (0.04 ± 0.02 events/min; $n = 20$ pups), long oscillations were most prominent and revealed a large amplitude of 461 ± 278.8 μV ($n = 51$). The average maximal frequency within these oscillations was 13.6 ± 6.8 Hz ($n = 51$). Simultaneous recordings of the FP and extracellular DC potential demonstrated that long oscillations are not related to spreading depressions, which were experimentally induced by local application of 1 M KCl (data not shown). Long oscillations did not affect the generation or properties of spindle bursts and gamma oscillations. Both activity patterns persisted after a long oscillation with similar amplitude, occurrence, duration, and frequency as before the prominent discharge. Similar to spindle bursts and gamma oscillations, long oscillations were accompanied by MUA (Fig. 2*C*) (supplemental Fig. 2*C*, available at www.jneurosci.org as supplemental material) and revealed an average cross-correlation coefficient of 0.79 ± 0.08 ($n = 3$ pups) (supplemental Fig. 2*D*, available at www.jneurosci.org as supplemental material).

These three activity patterns could be reliably recorded in urethane-anesthetized as well as in non-anesthetized rats and showed very similar properties in both experimental conditions (supplemental Table 1, available at www.jneurosci.org as supplemental material), indicating that these spontaneous patterns represent anesthesia-independent distinct oscillatory activities in neonatal rat S1. These patterns were further analyzed in their spatiotemporal properties, synchronization pattern, and developmental profile.

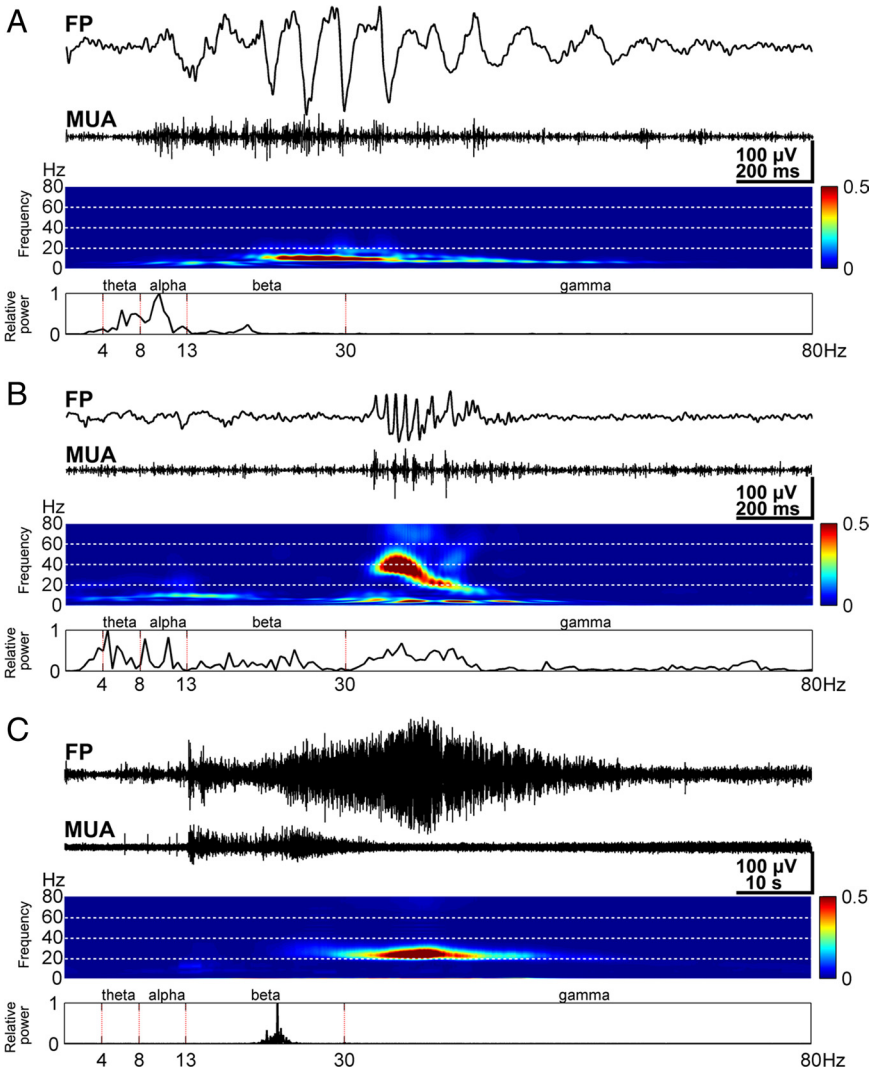

Figure 2. Properties of spindle bursts, gamma oscillations, and long oscillations. ***A***, Characteristic spindle burst recorded in S1 of a P1 rat (top) and corresponding MUA after 200 Hz high-pass filtering (below). Note the correlation between spindle burst and MUA. Color-coded frequency plot shows the wavelet spectrum of the field potential recording at identical timescale. Fast Fourier transformation (FFT) of the field potential recording illustrating the relative power of the displayed spindle burst with a maximal frequency at 10 Hz (bottom). ***B***, Characteristic gamma oscillation (top) recorded in the S1 of a P3 rat and corresponding MUA (below). Wavelet and FFT spectrum reveal prominent gamma activity between 30 and 50 Hz. ***C***, Characteristic long oscillation (top) recorded in S1 of a P6 rat and corresponding MUA (below). Color-coded wavelet spectrum and FFT (bottom) of the field potential recording display a narrow peak at 23 Hz. Note strong MUA at the onset of the long oscillation and different timescale compared with ***A*** and ***B***.

Spindle bursts synchronize neonatal cortical activity in a column-like pattern

Spindle bursts represent the dominant spontaneous activity pattern in the S1 of newborn rodents (Khazipov et al., 2004; Minlebaev et al., 2007). The spatiotemporal properties of spindle bursts were analyzed by field potential recordings in S1 at multiple stereotaxic coordinates ranging from 0 to 3 mm posterior to bregma and from 1 to 4.5 mm lateral to midline (Paxinos et al., 1991). Although spindle bursts could be recorded at all investigated 94 coordinates (50 pups), their properties were dependent on the site of recording in S1 (Fig. 3*A*). Spindle bursts recorded in the barrel field (0–2.5 mm posterior to bregma and 2.5–4.5 mm from the midline) occurred more frequently (6.2 ± 3.9 bursts/min; $n = 64$ stereotaxic coordinates; $p < 0.001$) (Fig. 3*Ai*) and had a larger amplitude (297.7 ± 271.5 μV; $n = 64$; $p < 0.05$) (Fig. 3*Aii*) and frequency within burst (9.9 ± 2.4 Hz; $n = 64$; $p < 0.01$)

(Fig. 3*Aiv*) but a shorter duration (1 ± 0.6 s; $n = 64$; $p < 0.001$) (Fig. 3*Aiii*) compared with spindle bursts recorded in S1 outside of the barrel field (occurrence, 3.5 ± 2.1 bursts/min; amplitude, 200 ± 168.5 μV; frequency within burst, 8.3 ± 1.9 Hz; duration, 2.2 ± 1 s; $n = 30$ coordinates). The different properties of spindle bursts recorded within or outside of the barrel field may reflect the unique structural and functional organization of the barrel cortex.

During the first postnatal week, spindle bursts revealed significant age-dependent alterations in their relative occurrence, amplitude, and maximal frequency (Fig. 3*B*). The average occurrence of spindle bursts increased significantly ($p < 0.001$) from 2.4 ± 1.6 bursts/min at P0–P1 ($n = 10$ pups) to 6.1 ± 2 bursts/min at P6–P7 ($n = 12$ pups) (Fig. 3*Bi*). Whereas the mean amplitude of spindle bursts also increased from 121.3 ± 85.4 μV at P0–P1 ($n = 157$ events from 10 pups) to 442 ± 455.6 μV at P6–P7 ($n = 275$ events from 12 pups) (Fig. 3*Bii*), their duration remained relatively constant during the first postnatal week (Fig. 3*iii*). The average maximal frequency within spindle burst significantly ($p < 0.001$) increased from 7.6 ± 2 Hz ($n = 157$) to 10.9 ± 4.9 Hz ($n = 275$) (Fig. 3*Biv*), and the relative power shifted from the theta toward beta band (Fig. 3*C*). In summary, these results demonstrate that spindle bursts occur more often and increase in amplitude and frequency during the first postnatal week, corresponding to a progressive maturation of the underlying neuronal networks and mechanisms for generation.

In the majority of the recordings (92%), spindle bursts were not restricted to one channel but rather occurred simultaneously at several neighboring recording sites of the 4 × 4-channel recording electrode (Fig. 4*Ai*) (supplemental Movie 2, available at www.jneurosci.org as supplemental material). To estimate the spatiotemporal dimension of the spindle burst-mediated functional coupling, the cross-correlation and coherence coefficients for all recording sites were calculated in relationship to one reference channel (Fig. 4*Aii*). In 51% of all recordings ($n = 663$ events from 49 pups), the spindle bursts were synchronized in a column-like pattern. The average cross-correlation (0.8 ± 0.05; $n = 48$ pups) and coherence coefficients (theta band, 0.85 ± 0.06; alpha band, 0.83 ± 0.05; beta band, 0.82 ± 0.06; $n = 48$ pups) of spindle bursts were significantly ($p < 0.001$) higher within a 200- to 400-μm-wide cortical column compared with activity recorded at more remote regions (>400 μm). Only 20% of the spindle bursts ($n = 268$ events from 38 pups) were synchronized within a horizontal column, and 21% of them ($n = 269$ events from 39 pups) appeared widely synchronized at all 16 recordings sites. The remaining 8% ($n = 105$ events from 28 pups) appeared very localized at only one or two recording sites.

Spindle bursts were not only synchronized within one hemisphere but surprisingly also across both hemispheres. Spontaneous activity was recorded simultaneously in both hemispheres at the same stereotaxic coordinates and depth (Fig. 4*Bi*). However, the amount of interhemispherical synchronization (Fig. 4*Bii*) was relative low (13.1 ± 9.2%; $n = 204$ events in 27 pups) and increased during the first postnatal week (Fig. 4*Biii*). Whereas in P0–P1 rats, only 4.7 ± 5.7% of all recorded spindle bursts ($n = 9$ events in 4 pups) occurred simultaneously in both hemispheres, the degree of interhemispherical synchronization progressively increased to 18.4 ± 9% in P6–P7 rats ($n = 95$ events in 10 pups).

Previous *in vitro* experiments in immature rat cerebral cortex demonstrated a horizontal propagation of activity over the somatosensory cortex (Yuste et al., 1995; Garaschuk et al., 2000; Peinado, 2001; Dupont et al., 2006; Sun and Luhmann, 2007). We calculated the onset delay of spindle bursts recorded at neighboring channels and could not detect a propagation of this type of spontaneous activity *in vivo*.

Our results demonstrate that nonpropagating spindle bursts intrahemispherically and interhemispherically synchronize the spontaneous activity in a 200- to 400-μm-wide column-like neocortical network.

Fast gamma oscillations are mainly confined to the barrel cortex in which they locally synchronize developing neuronal networks

Gamma oscillations significantly differed in their spatiotemporal organization from spindle bursts (data above) (supplemental Fig. 1, available at www.jneurosci.org as supplemental material). In contrast to the ubiquitary distribution of spindle bursts in the entire S1, gamma oscillations were confined to a cortical region corresponding to the barrel field (Fig. 5*A*). Gamma oscillations could be recorded at 48 of 64 stereotaxic coordinates located within the barrel cortex but at only 6 of 30 coordinates outside the barrel field. However, gamma oscillations recorded within the barrel field were relatively uniform in their occurrence (Fig. 5*Ai*), amplitude (Fig. 5*Aii*), duration (Fig. 5*Aiii*), and frequency (Fig. 5*Aiv*). Similar to spindle bursts, gamma oscillations also revealed age-dependent alterations during the first postnatal week. Their occurrence significantly ($p < 0.01$) increased from 1.9 ± 1.6 oscillations/min ($n = 5$ pups) at P0–P1 to 6.9 ± 3.4 oscillations/min ($n = 11$ pups) at P6–P7 (Fig. 5*Bi*). Furthermore, the amplitude of gamma oscillations also significantly ($p < 0.001$) increased from 95 ± 79 μV ($n = 43$ events from 5 pups) at P0–P1 to 154.8 ± 150.2 μV ($n = 190$ events from 11 pups) at P6–P7 (Fig. 5*Bii*). Their duration significantly ($p < 0.001$) increased from 0.13 ± 0.04 s ($n = 43$) at P0–P1 to 0.3 ± 0.2 s ($n = 190$) at the end of the first postnatal week (Fig. 5*Biii*). In contrast, the average maximal frequency of gamma oscillations remained almost unchanged from P0 to P7 (Fig. 5*Biv*).

The cross-correlation and coherence analyses of gamma oscillations recorded with the 4 × 4 electrode array revealed a rather local organization and synchronization of this activity pattern in the barrel cortex. The majority of gamma oscillations (74.9% of 962 events from 32 pups) were restricted to one or two and seldom to three recording sites (Fig. 6*Ai*) (supplemental Movie 3, available at www.jneurosci.org as supplemental material). The gamma activity was highly synchronized at these neighboring recording sites as illustrated in the cross-correlation plot (Fig. 6*Aii*). Synchronized gamma oscillations were restricted to a local neuronal network of ~200 μm in diameter. A small number of gamma oscillations (6.2 ± 6.9%; $n = 66$ events in 20 pups) revealed a synchronization between both hemispheres (Fig. 6*B*). The degree of interhemispherical synchronization increased with age from 2.6 ± 4.7% at P0–P2 ($n = 6$ in 5 pups) to 10.9 ± 9.2% at P6–P7 ($n = 41$ in 7 pups). However, these developmental changes were not significant at the $p < 0.05$ level (Fig. 6*C*). Furthermore, we never observed propagation of gamma oscillations over S1.

These data indicate that local neuronal networks in the developing barrel field of S1 are highly synchronized by spontaneous oscillatory gamma activity.

Propagating long oscillations synchronize spontaneous activity over wide cortical regions

In contrast to spindle bursts and gamma oscillations, long oscillations propagated over wide cortical regions and thus could be recorded in the entire S1. Our data indicate that long oscillations,

similar as spindle bursts, are not a specific activity pattern of the developing barrel field but rather of the whole somatosensory or even entire cerebral cortex. Their occurrence (barrel field, 0.04 ± 0.02 oscillations/min, $n = 14$ stereotaxic coordinates; non-barrel field, 0.05 ± 0.02 oscillations/min, $n = 10$ stereotaxic coordinates) (Fig. 7*Ai*), amplitude (barrel field, 533.9 ± 350.6 μV, $n = 14$; non-barrel field, 407.4 ± 311.9 μV, $n = 10$) (Fig. 7*Aii*), duration (barrel field, 49.2 ± 13.9 s, $n = 14$; non-barrel field, 56.4 ± 21.2 s, $n = 10$) (Fig. 7*Aiii*), and mean maximal frequency within oscillation (barrel field, 11.8 ± 6 Hz, $n = 14$; non-barrel field, 13 ± 6.9 Hz, $n = 10$) (Fig. 7*Aiv*) showed no significant differences when analyzed separately for the barrel field and the remaining part of S1.

As the other spontaneous activity patterns, long oscillations also revealed significant age-dependent alterations during the first postnatal week (Fig. 7*B*). Their occurrence increased progressively ($p < 0.01$) from 0.03 ± 0.015 oscillations/min ($n = 6$ pups) at P0–P1 to 0.06 ± 0.002 oscillations/min at P6–P7 ($n = 4$ pups) (Fig. 7*Bi*). Similarly, the maximal amplitude of long oscillations increased significantly ($p < 0.001$) from 190.5 ± 142.4 μV ($n = 9$ events from 6 pups) at P0–P1 to 586.7 ± 302.7 μV ($n = 16$ events from 4 pups) at P6–P7 (Fig. 7*Bii*), and their frequency also increased significantly ($p < 0.001$) during the first postnatal week (P0–P1, 6.5 ± 1.4 Hz, $n = 9$; P6–P7, 21.7 ± 4.7 Hz, $n = 16$) (Fig. 7*Biv*). Only the duration of long oscillations remained relatively constant between P0 and P7 (Fig. 7*Biii*).

Long oscillations also differed from spindle bursts and gamma oscillations in their synchronization pattern. The majority of long oscillations (76.5% of 51 events from 20 pups) occurred simultaneously at all recoding sites (Fig. 8*Ai*) (supplemental Movie 4, available at www.jneurosci.org as supplemental material). The synchronization of neuronal activity over a large cortical area (~600–800 μm) was demonstrated by the high cross-correlation as well as coherence coefficients that were calculated for a large fraction of the recording channels (Fig. 8*Aii*). Long oscillations were also characterized by their propagation pattern (Fig. 8*B*). A mediotemporal spread of long oscillatory activity with an average speed of 25.1 ± 16.4 μm/s could be observed in 11 of 39 events (28.2%) and 35.9% of the long oscillations propagated in the temporomedial direction at 28.1 ± 10 μm/s (Fig. 8*B*). The

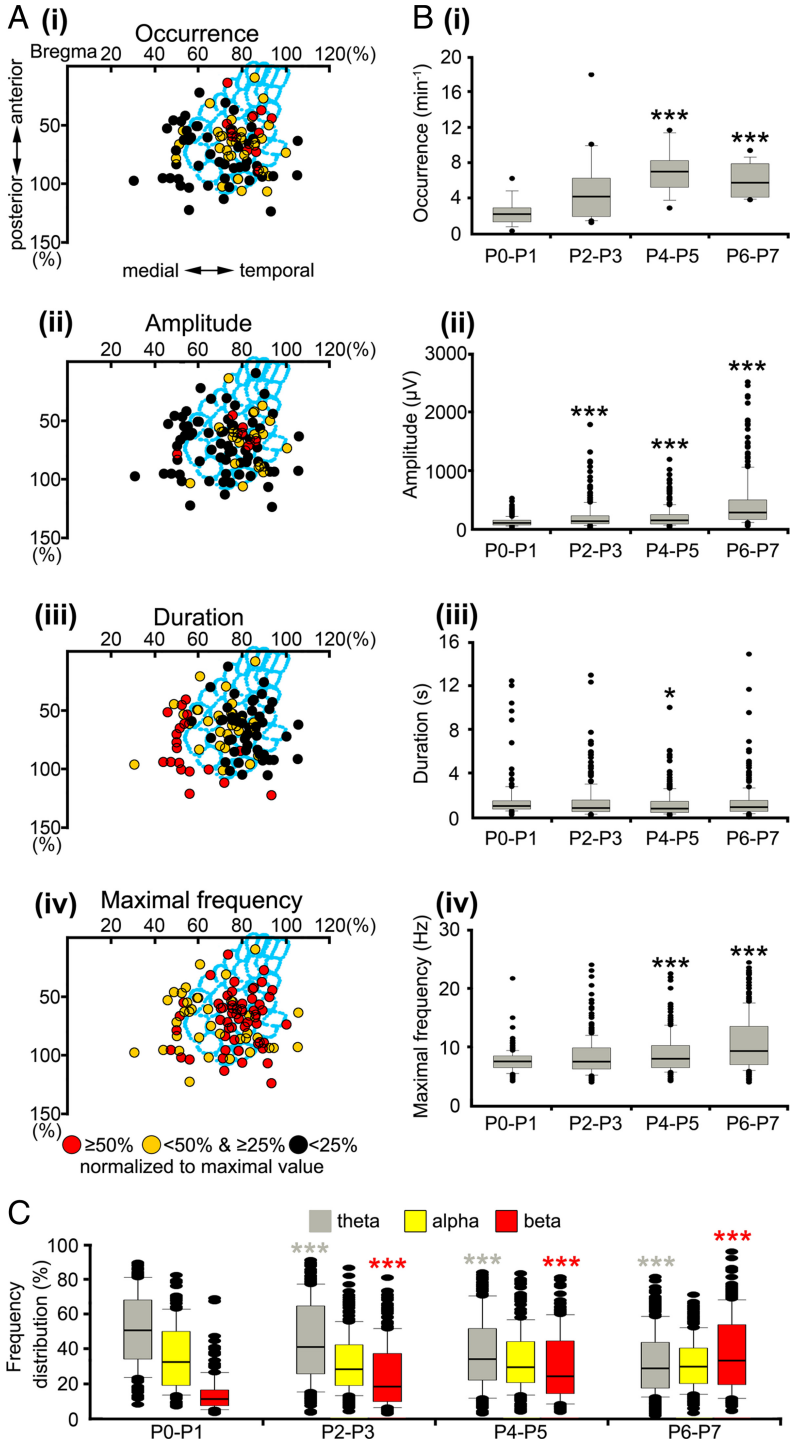

Figure 3. Spatiotemporal properties and developmental profile of spindle burst activity in neonatal rat S1. ***A***, Spatial distribution of spindle bursts recorded at 94 recording sites in 50 P0–P7 rats. The stereotaxic coordinates of the recording sites were determined in relationship to bregma and midline in each pup and are displayed normalized to the lateral and posterior borders (100%) of the barrel field (light blue). The occurrence (***i***), amplitude (***ii***), duration (***iii***), and maximal frequency within burst (***iv***) of each spindle burst were normalized to the maximal value and displayed in color code. Spindle bursts recorded within the barrel field revealed a higher occurrence, larger amplitude, lower duration, and higher frequency when compared with spindle bursts recorded outside the barrel field. ***B***, Developmental profile of the spindle burst activity in P0–P7 rat S1. Box plots displaying the progressive increase in the occurrence (***i***), amplitude (***ii***), and maximal frequency within burst (***iv***) during the first postnatal week. The average spindle burst duration reveals no major change during early development (***iii***). ***C***, Spindle bursts gradually shift toward faster frequency bands with a relatively stable contribution of alpha activity. In ***B*** and ***C***, the values correspond to spindle bursts recorded from 10 P0–P1 pups, 16 P2–P3 pups, 12 P4–P5 pups, and 12 P6–P7 pups. Data are expressed as box plots, and asterisks mark significant differences compared with the P0–P1 group (*$p < 0.05$, **$p < 0.01$, ***$p < 0.001$, Mann–Whitney–Wilcoxon test).

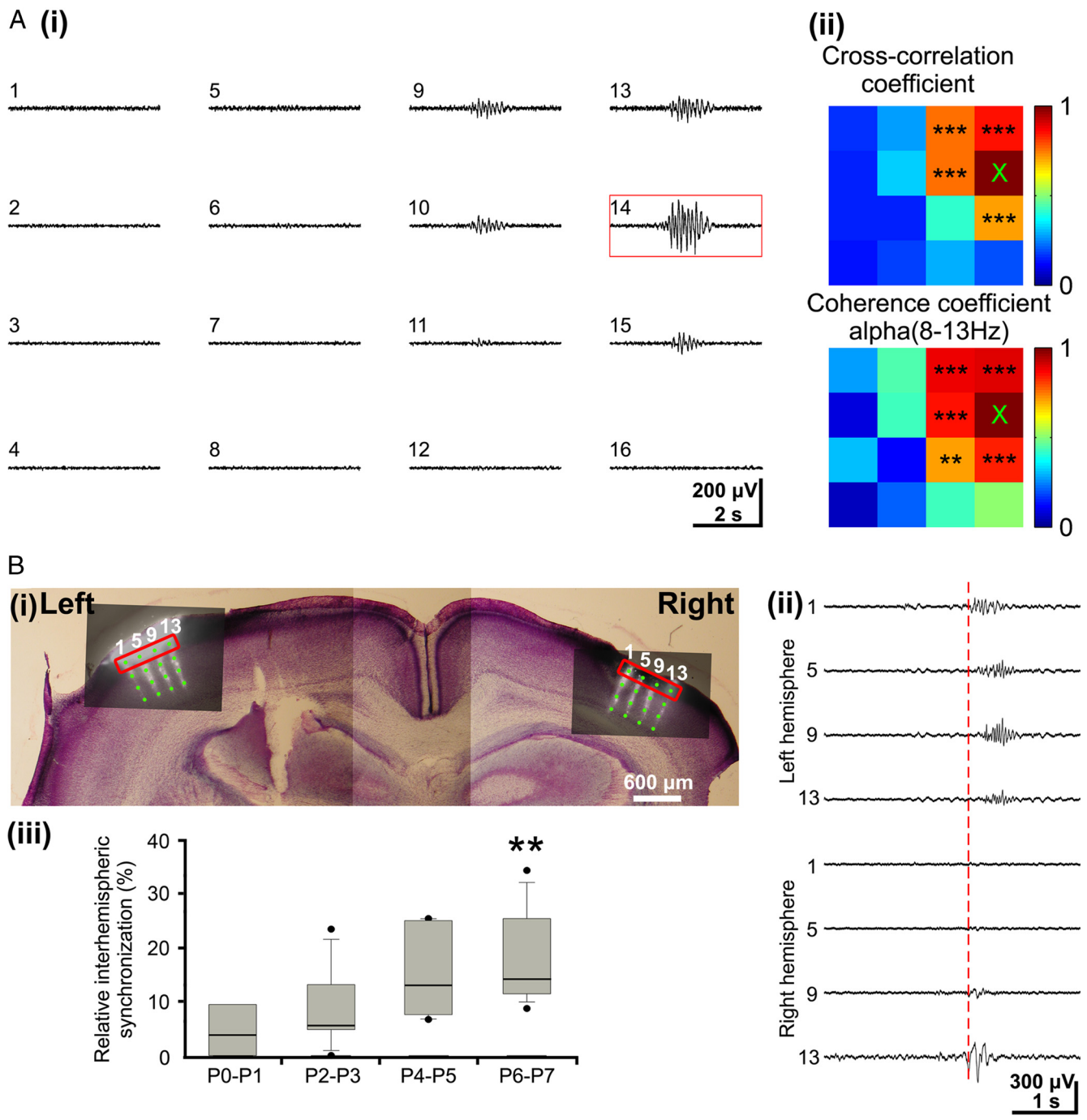

Figure 4. Intrahemispheric and interhemispheric synchronization of spindle bursts in the neonatal rat barrel cortex. ***A***, ***i***, Simultaneous field potential recordings from a P1 rat with the 4 × 4-channels electrode array (interelectrode distance of 200 μm) demonstrating simultaneous spindle burst activity at multiple recording sites. ***ii***, Color-coded plots of maximal cross-correlation and coherence coefficients calculated for the 4 × 4 recordings shown in ***i***. Channel number 14 (red box in ***i*** and × in plots) was used as reference channel, and the coherence was calculated for the dominant alpha frequency band. Note the columnar-like distribution of the significant cross-correlation and coherence coefficients marked by asterisks. ***B***, ***i***, Digital photomontage of a 200-μm-thick Nissl-stained coronal slice reconstructing the position of the two DiI-covered 4 × 4-channels electrode arrays inserted at the same stereotaxic coordinates in both hemispheres of a P7 rat. ***ii***, Simultaneous field potential recordings from the upper channels of the electrode arrays (marked by red boxes in ***i***). Note synchronized spindle bursts activity at homotopic recording sites in both hemispheres (channel 1 left vs channel 13 right hemisphere). The red dotted line marks the onset of interhemispheric spindle bursts. ***iii***, Age-dependent increase in interhemispheric synchronization of spindle burst activity from P0 to P7 in rat barrel cortex. Box plot displaying the relative amount of spindle bursts occurring simultaneously on both hemispheres in relationship to the total amount of spindle bursts. The displayed values were obtained in 4 P0–P1 pups, 7 P2–P3 pups, 6 P4–P5 pups, and 10 P6–P7 pups.

remaining 35.9% of the long oscillations did not propagate but occurred highly synchronized at all recording sites.

These results indicate that long oscillations are a distinct propagating pattern of activity that synchronizes the developing neocortical network over large distances.

All three patterns of cortical synchronized oscillations can be elicited by activation of the sensory input

Activation of the periphery has been reported previously to trigger network oscillations in the primary visual (Hanganu et al.,

2006) and somatosensory (Khazipov et al., 2004) cortex of newborn rats. To address the question whether the three different activity patterns can be also elicited by activation of the peripheral sensory input, field potentials were recorded with the 4 × 4 electrode array in the barrel cortex after stimulation of all whiskers either by tactile stimulation or by electrical stimulation of the entire whisker pad (Fig. 9*Ai*). Electrical stimulation using a bipolar electrode elicited in 10 of 10 pups in the contralateral barrel cortex a robust initial cortical response with a delay of 40.3 ± 11.2 ms and an average amplitude of 536.8 ± 435.1 μV (n = 137 events in 10 pups) (Fig. 9*Aii*, *Aiii*). In contrast, stimulation of the whisker pad evoked in the ipsilateral barrel field a very small response in one rat and no response in nine pups. In 88% of the 140 recordings, the direct response in the contralateral barrel cortex was often followed by a late oscillatory component. Both spindle bursts (Fig. 9*Aii*) and gamma oscillations (Fig. 9*Aiii*) could be evoked by whisker stimulation in 87.5 ± 11.8% (n = 125 events in 10 pups) and 62.3 ± 21.4% (n = 44 events in 5 pups) of the experiments, respectively. The evoked spindle bursts started 228.4 ± 145 ms after stimulation and showed similar properties (average maximal frequency, 9.9 ± 4 Hz; amplitude, 670 ± 490.2 μV; n = 125 in 10 pups) as the spontaneous spindle bursts. Their occurrence was strongly correlated with the MUA (mean cross-correlation coefficient, 0.53 ± 0.2; n = 9 pups) (Fig. 9*Aii*), and their synchronization pattern reflected the columnar organization as described for the spontaneous spindle bursts (Fig. 9*Bi*). Similar results could be obtained for the stimulus-evoked gamma oscillations. They started 410.5 ± 347.7 ms after stimulation, and their average maximal frequency (38.2 ± 7.2 Hz; n = 44 in 5 pups) and amplitude (557.7 ± 608.7 μV; n = 44 in 5 pups) were similar to those of the spontaneous gamma events. Furthermore, the evoked gamma oscillations strongly correlated with the MUA as shown by the cross-correlation analyses (mean cross-correlation coefficient, 0.77 ± 0.04; n = 5 pups) and synchronized rather small local networks of ~200 μm in diameter (Fig. 9*Bii*). Beside electrical stimulation, tactile stimulation of all whiskers evoked in a very similar manner spindle bursts and gamma oscillations in 82.7 ± 19% (n = 92 from 111 trials) and 77.1 ± 21.4% (n = 55 from 71 trials) of the experiments, respectively. Although this multiwhisker stimulation protocol elicited large-scale activity in the barrel cortex, the oscillatory patterns were again locally synchronized in 200- to 400-μm-wide column-like networks (data not shown).

Although spindle bursts and gamma oscillations could be elicited by single electrical stimulation of the whisker pad, this protocol failed to evoke long oscillations in all investigated animals (n = 10).

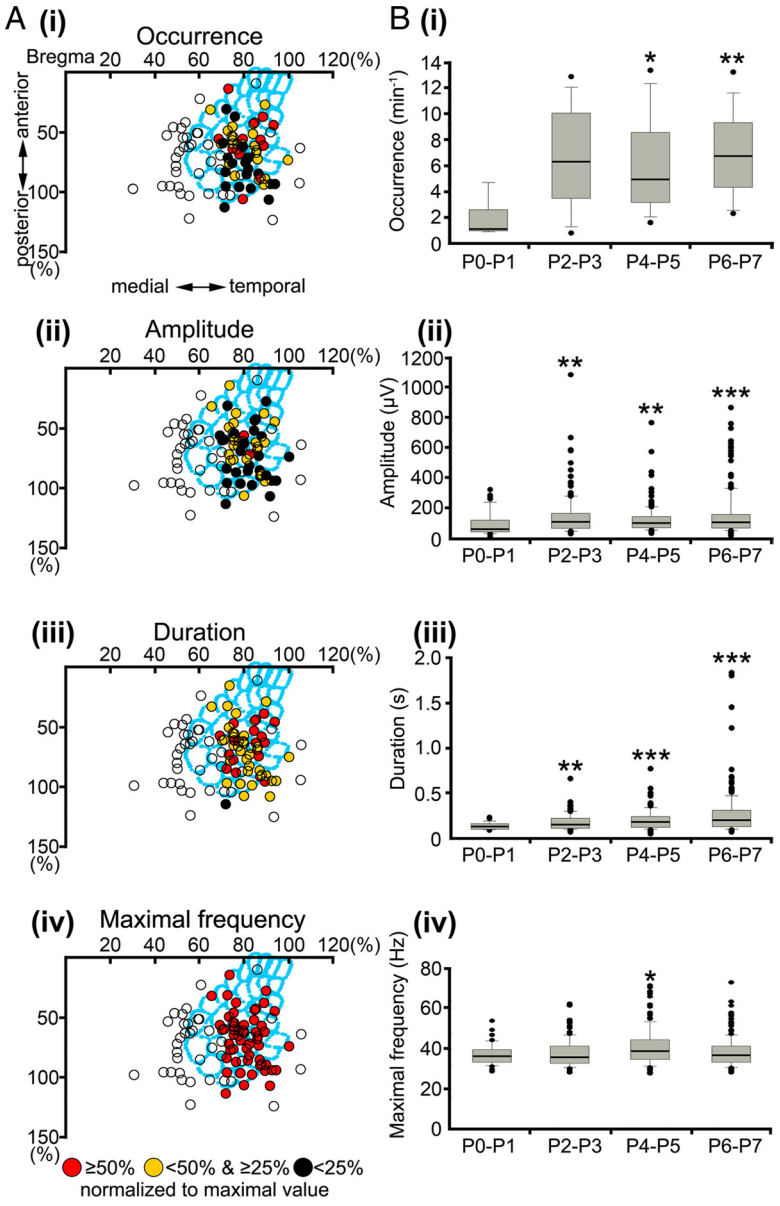

Figure 5. Spatiotemporal properties and developmental profile of gamma oscillations. ***A***, Spatial distribution of gamma activity recorded at 54 recording sites in 32 newborn rats. Note that gamma oscillations are mainly restricted to the cortical region corresponding to the barrel field in S1. Open circles correspond to stereotaxic coordinates in which gamma oscillations could not be recorded. ***B***, Developmental profile of the gamma oscillations in P0–P7 rat S1. Box plots illustrate age-dependent alterations in the occurrence (***i***), amplitude (***ii***), duration (***iii***), and maximal frequency (***iv***) during the first postnatal week. The displayed values correspond to gamma oscillations recorded in 5 P0–P1 pups, 8 P2–P3 pups, 8 P4–P5 pups, and 11 P6–P7 pups. For additional details, see Figure 3.

However, long oscillations could be evoked by repetitive tactile stimulation of all whiskers (10 or 11 times at ~1 Hz) in four of six pups (Fig. 9*C*). These evoked long oscillations started at 14.7 ± 10.3 s after the last tactile stimulus, lasted 52 ± 4.3 s, and showed a mean amplitude of 447.7 ± 210.3 μV and an averaged maximal frequency of 17.6 ± 5.1 Hz (n = 4 events in 4 pups).

The relative contribution of the sensory input to the generation of neocortical oscillatory activity patterns was also investigated by silencing the sensory periphery. A temporal peripheral deafferentation of the whiskers was induced by injecting 2% lidocaine subcutaneously into the face just adjacent to the whisker pad as described previously (Krupa et al., 1999; Shaw and Liao, 2005). The activity persisted after lidocaine injection, but the occurrence of spindle bursts (control, 10.7 ± 3.3 bursts/min; lidocaine, 4.8 ± 3.6 bursts/

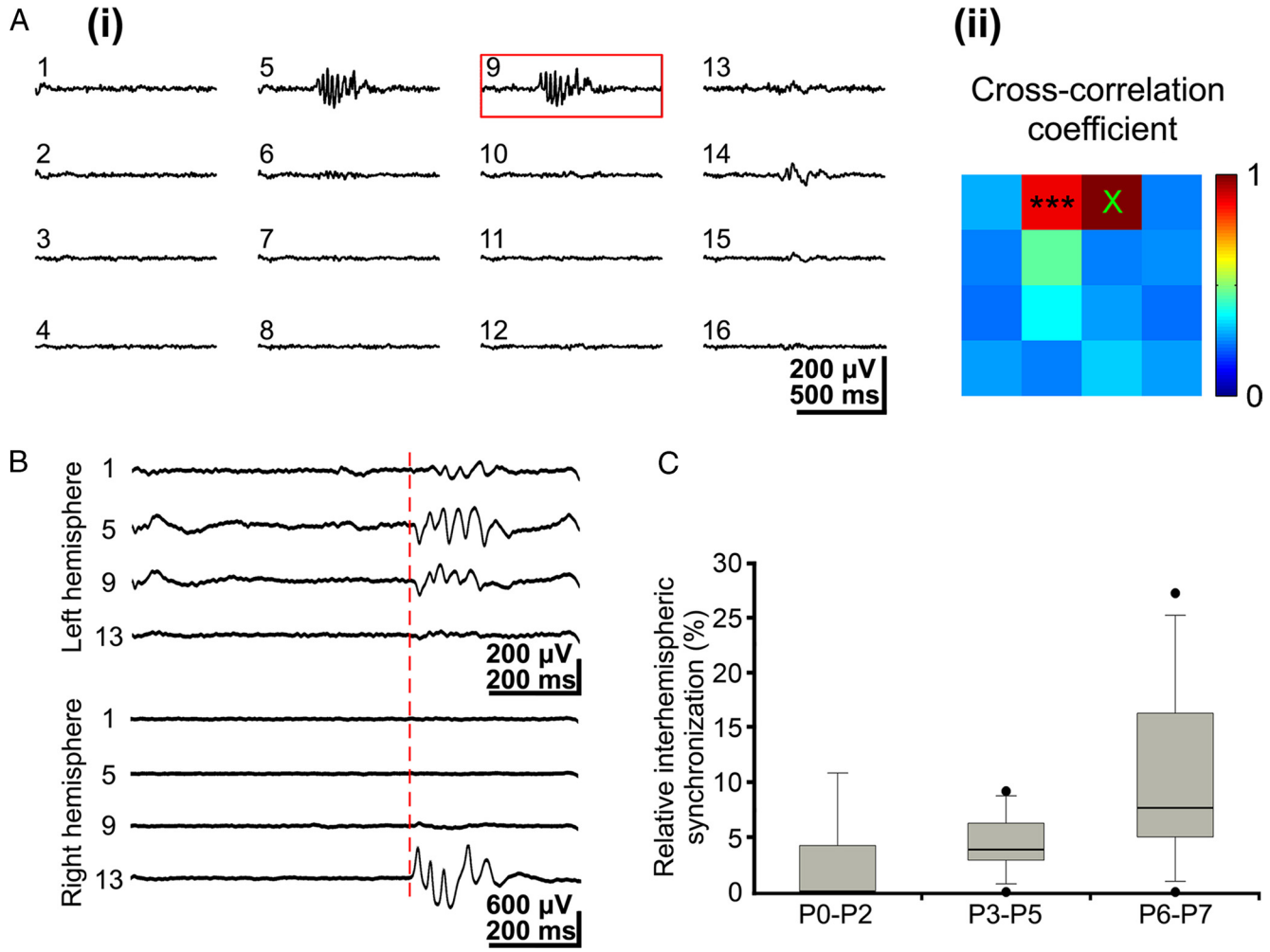

Figure 6. Intrahemispheric and interhemispheric synchronization of gamma oscillations. ***A***, ***i***, Simultaneous field potential recordings in a P3 rat somatosensory cortex showing gamma oscillations at a few recording sites. ***ii***, Color-coded plot of maximal cross-correlation coefficients calculated for the 16 recordings shown in ***i*** with channel 9 as a reference channel (red box in ***i***). Note spatial restriction of synchronized gamma activity to only two recording sites. ***B***, Simultaneous gamma oscillations recorded at homotopic sites in left and right hemispheres in a P3 rat. The red dotted line marks the onset of synchronized interhemispheric gamma oscillations. ***C***, Incidence of interhemispheric gamma synchronization during the first postnatal week. The values correspond to gamma oscillations recorded in five P0–P2 pups, eight P3–P5 pups, and seven P6–P7 pups.

min; $p < 0.01$; $n = 6$ pups) and gamma oscillations (control, 8.9 ± 3.3 oscillations/min; lidocaine, 4 ± 2.7 oscillations/min; $p < 0.05$; $n = 6$ pups) significantly decreased in the contralateral barrel cortex (Fig. 9*D*). The amplitude of spindle bursts (control, 344.1 ± 273.8 µV, $n = 60$ events from 6 pups; lidocaine, 321.6 ± 191.5 µV, $n = 44$ events from 6 pups) and gamma oscillations (control, 164.2 ± 120 µV, $n = 60$ events from 6 pups; lidocaine, 154.4 ± 81.1 µV, $n = 51$ events from 6 pups) were not affected by the functional deafferentation. Similarly, lidocaine did not affect the frequency of contralateral spindle bursts (control, 8.4 ± 3.4 Hz, $n = 60$; lidocaine, 7.6 ± 2.6 Hz, $n = 44$) and gamma oscillations (control, 38.3 ± 7 Hz, $n = 60$; lidocaine, 38 ± 6.3 µV, $n = 51$). Only the duration of spindle bursts decreased significantly ($p < 0.05$) from 1.1 ± 1.5 s ($n = 60$) to 0.75 ± 1.1 s ($n = 44$) after lidocaine injection, whereas the short duration of gamma oscillations remained unchanged (control, 0.23 ± 0.16 s, $n = 60$; lidocaine, 0.19 ± 0.12 s, $n = 51$). Furthermore, the properties of spindle bursts and gamma oscillations in the ipsilateral barrel cortex remained unaffected after lidocaine injection (Fig. 9*D*). The low occurrence of long oscillations (~1 per 20 min) circumvented a reliable conclusion whether functional deafferentation affected also this activity pattern.

Summarizing, these results indicate that whisker activation can trigger both neonatal spindle bursts and gamma oscillations. The large amount of oscillatory activity persisting after functional deafferentation indicates that the peripheral sensory input is clearly not the only mechanism to trigger these activity patterns.

Neocortical circuitry and pharmacological profile

The neocortical network underlying the spindle burst activity was studied by the use of a one-shank 16-channel electrode covering the entire cortical depth of P0–P2 pups (supplemental Fig. 3, available at www.jneurosci.org as supplemental material). Field potentials (left traces in supplemental Fig. 3, available at www.jneurosci.org as supplemental material), corresponding CSD (middle traces), and averaged CSD plots (right traces) demonstrated two different depth profiles. In 61% of the 215 spindle bursts recorded in two rats, the CSD profile revealed a clear participation of the subplate with a clear sink located in the subplate and the corresponding source in the cortical plate above (averaged CSD in supplemental Fig. 3*A*, available at www.jneurosci.org as supplemental material). These results support our previous *in vitro* observations that the subplate plays an important role in the generation of oscillatory network activity in the newborn rat neocortex (Dupont et al., 2006). Ad-

ditional support for this hypothesis comes from our analyses of the field potential recordings in the cortical plate and simultaneous recordings of the MUA in the subplate. These experiments demonstrated that the MUA in the subplate preceded the negative peaks of each oscillatory cycle in the spindle bursts on average by 13.8 ± 14.3 ms (n = 281 cycles from 80 spindle bursts recorded in 6 pups) (supplemental Fig. 6*Ai*, available at www.jneurosci.org as supplemental material). The MUA in the subplate also correlated with the MUA in the cortical plate according to the cross-correlation histogram (supplemental Fig. 6*Aii*, *Aiii*, available at www.jneurosci.org as supplemental material). These data are in agreement with previous structural and functional observations in newborn rat cerebral cortex by Molnár et al. (1998, 2003), demonstrating an early innervation of the subplate by thalamocortical afferents. Our present report shows the contribution of the thalamic input for the generation of cortical spindle bursts. A different depth profile could be observed in the remaining spindle burst recordings. In 39% of the 215 spindle bursts recorded in two pups, the activity was restricted to the upper cortical layers without any detectable participation of the subplate (supplemental Fig. 3*B*, available at www.jneurosci.org as supplemental material). These data indicate that local neuronal networks in the cortical plate and layers V/VI are also capable to generate spindle burst activity as we have demonstrated previously with the multielectrode array technology (MEA chip) in 1000-μm-thick neocortical slices from newborn mice (Sun and Luhmann, 2007). Local nonpropagating spontaneous oscillations with an average frequency of 15.6 Hz and duration of 1.7 s were localized in the cortical plate and synchronized the activity in a ~200-μm-wide column-like network (Sun and Luhmann, 2007).

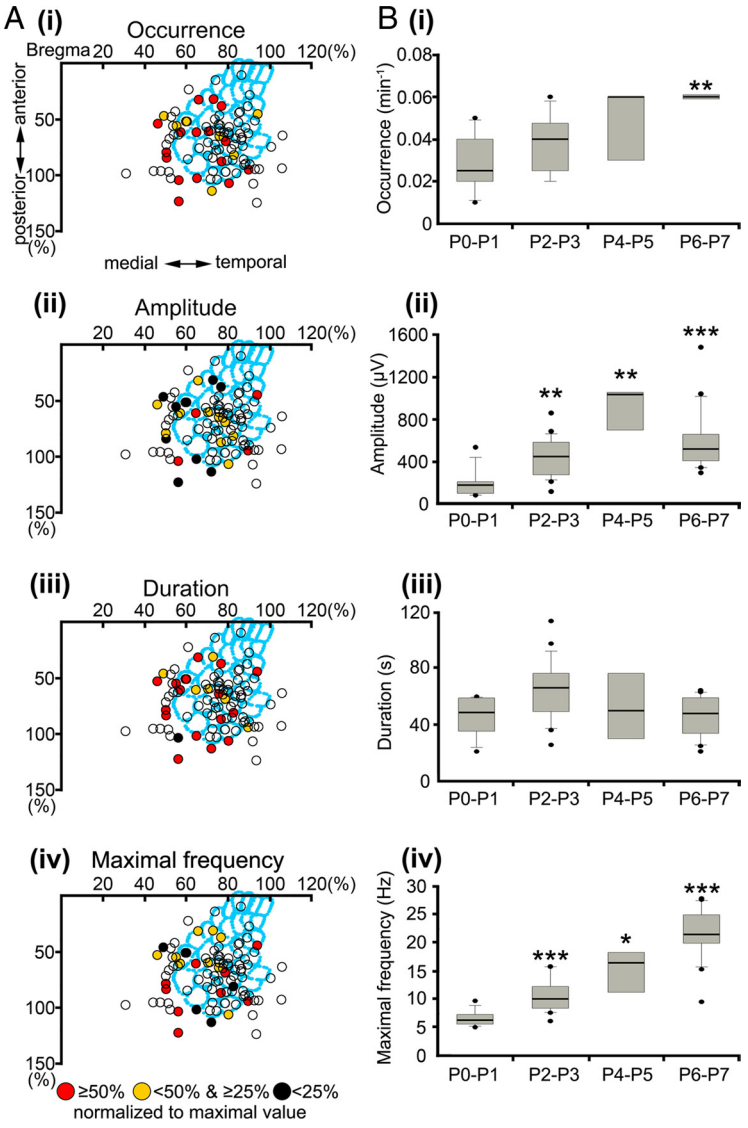

Figure 7. Spatiotemporal properties and developmental profile of long oscillations. ***A***, Spatial distribution of long oscillations recorded at 24 recording sites in 20 newborn rats. Note the relatively low incidence of long oscillations in the barrel field. ***B***, Developmental profile of long oscillations in P0–P7 rat S1. Box plots illustrate age-dependent alterations in the occurrence (***i***), amplitude (***ii***), duration (***iii***), and maximal frequency (***iv***) during the first postnatal week. Long oscillations reveal a significant increase in frequency during the first postnatal week. The values correspond to long oscillations recorded in six P0–P1 pups, seven P2–P3 pups, three P4–P5 pups, and four P6-P7 pups. For additional details, see Figure 3.

CSD were also used to study the neocortical circuitry underlying the gamma oscillations (supplemental Fig. 4, available at www.jneurosci.org as supplemental material) and the long oscillations (supplemental Fig. 5, available at www.jneurosci.org as supplemental material). In 70% of the 86 gamma oscillations recorded in two pups, the CSD profile demonstrated a sink in the subplate and the corresponding source in the cortical plate above (averaged CSD in supplemental Fig. 4*A*, available at www.jneurosci.org as supplemental material). In the remaining 30% of the gamma oscillations, the activity was restricted to the upper cortical layers (supplemental Fig. 4*B*, available at www.jneurosci.org as supplemental material). The MUA in the subplate also preceded the negative peaks of each oscillatory cycle in the gamma oscillation by 4.3 ± 4.7 ms (n = 32 cycles from 19 gamma oscillations recorded in two pups) (supplemental Fig. 6*Bi*, available at www.jneurosci.org as supplemental material) and the MUA in the subplate correlated with the MUA in the cortical plate according to the cross-correlation histogram (supplemental Fig. 6*Bii*, *Biii*, available at www.jneurosci.org as supplemental material), indicating that the subplate also participates in the generation of gamma oscillations in the newborn rat cerebral cortex. Finally, CSDs were also used to study the circuitry underlying the generation of the long oscillations (supplemental Fig. 5, available at www.jneurosci.org as supplemental material). The CSD profiles calculated from three long oscillations recorded in two rat pups revealed in two cases a clear participation of the subplate with a clear sink located in the subplate and the corresponding source in the cortical plate above (averaged CSD in supplemental Fig. 5*A*, available at www.jneurosci.org as supplemental material) and, in one case, oscillatory activity mostly restricted to the upper cortical layers (supplemental Fig. 5*B*, available at www.jneurosci.org as supplemental material).

The mechanisms underlying the early network oscillations

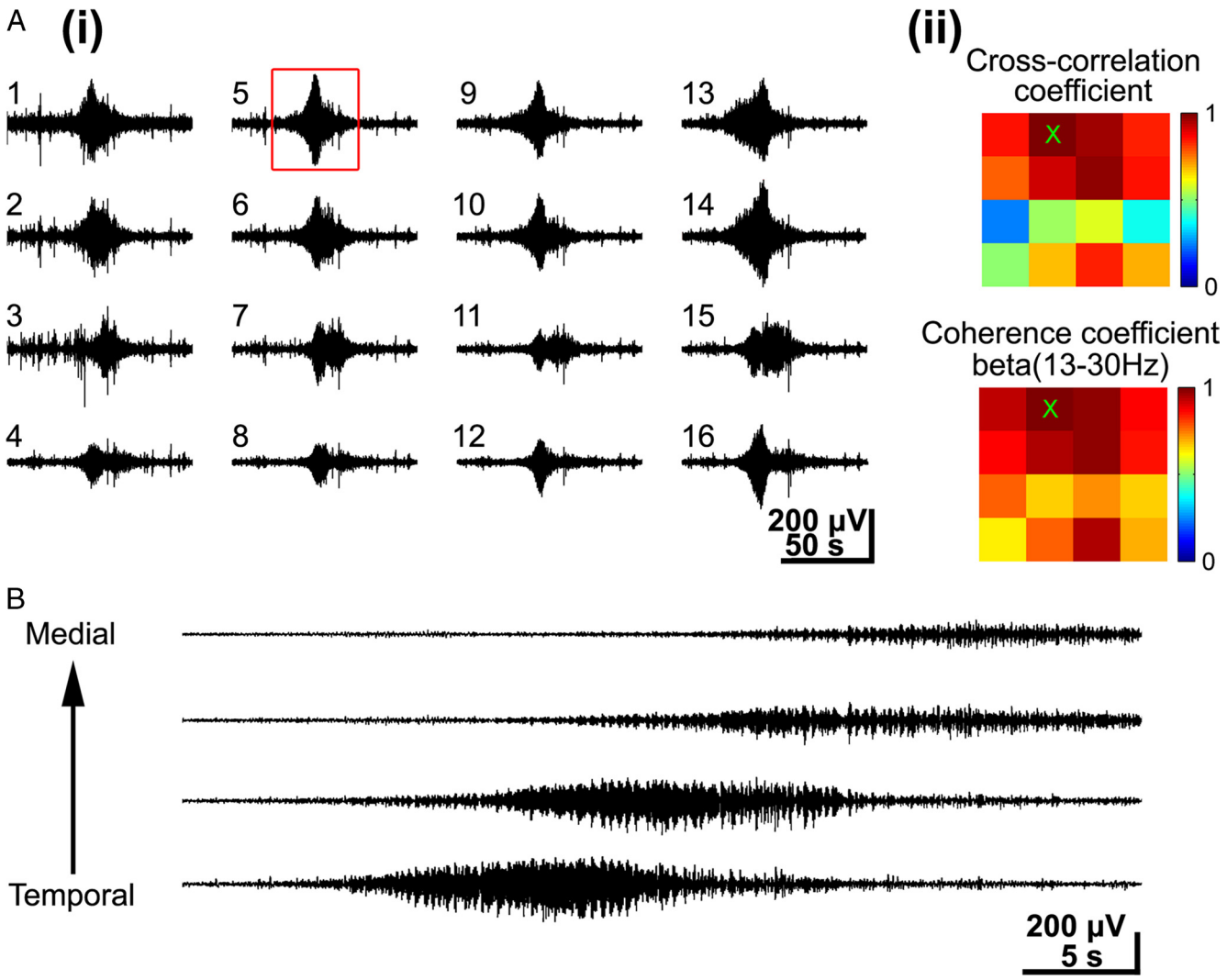

Figure 8. Synchronization and horizontal propagation of long oscillations. ***A***, ***i***, Simultaneous recordings of long oscillations in the barrel cortex of a P6 rat. Note prominent expression of long oscillations at all recording sites. ***ii***, Color-coded plot of maximal cross-correlation and coherence coefficients calculated for the 16 recordings shown in ***i*** using channel 5 (red box in ***i***, and × in ***ii***) as a reference channel. The coherence was calculated for the dominant beta frequency band. Note the wide-spread synchronization of long oscillations as indicated by the large number of recording sites with high cross-correlation and coherence coefficients. ***B***, Simultaneous recordings of long oscillations at four recording sites located at the same cortical depth in the barrel field of a P6 rat.

were further assessed by pharmacological manipulation of chemical and electrical synaptic transmission within S1 of the P0–P2 rat *in vivo*. We focused on the pharmacological profile of spindle bursts (supplemental Fig. 7*A*, available at www.jneurosci.org as supplemental material) and gamma oscillations (supplemental Fig. 7*B*, available at www.jneurosci.org as supplemental material), because the very rare occurrence of long oscillations precluded a reliable investigation of their pharmacological properties. Drugs were applied on the surface of the cerebral cortex near the recording site. Control experiments with application of the vehicle (200 nl of ACSF) without any drug did not cause any alterations in the spindle burst ($n = 17$ animals) or gamma oscillation pattern ($n = 9$) demonstrated that this application procedure by itself did not cause any changes in the neuronal network activity. In contrast, application of the NMDA receptor antagonist APV (100 μM, 200 nl) on the cortical surface caused a significant decrease in the occurrence of spindle bursts to 56.4 ± 17.8% ($n = 12$ pups; $p < 0.001$) and of gamma oscillations to 36.1 ± 27.3% ($n = 6$; $p < 0.01$). Blockade of gap junctional coupling by application of carbenoxolone (100 μM, 200 nl) significantly reduced the occurrence of spindle bursts to 57.5 ± 29.9% ($n = 8$ pups; $p < 0.001$) and of gamma oscillations to 48.4 ± 17.1% ($n = 6$; n <0.01). To address the question whether a drug applied on the cortical surface actually reaches the underlying neocortical network, 2% lidocaine (200 nl) was applied in an identical manner on the surface of the cortex near the recording electrode. Spindles bursts and gamma oscillations were inhibited by lidocaine in their occurrence to 11.5 ± 10.6 and 1.6 ± 4.6%, respectively (supplemental Fig. 7, available at www.jneurosci.org as supplemental material), indicating that this method allows pharmacological intervention in the developing rat cerebral cortex.

Discussion

Coordinated network activity is a hallmark of developing neuronal networks in a variety of species, including humans (for review, Torborg and Feller, 2005; Khazipov and Luhmann, 2006; Vanhatalo and Kaila, 2006). In the present study, we investigated the properties and mechanisms of coordinated activity patterns in S1 of the newborn rat *in vivo* using multielectrode recording techniques. We demonstrate for the first time the following: (1) the neonatal rat S1 generates under *in vivo* conditions three distinct oscillatory activity patterns; (2) these activity pat-

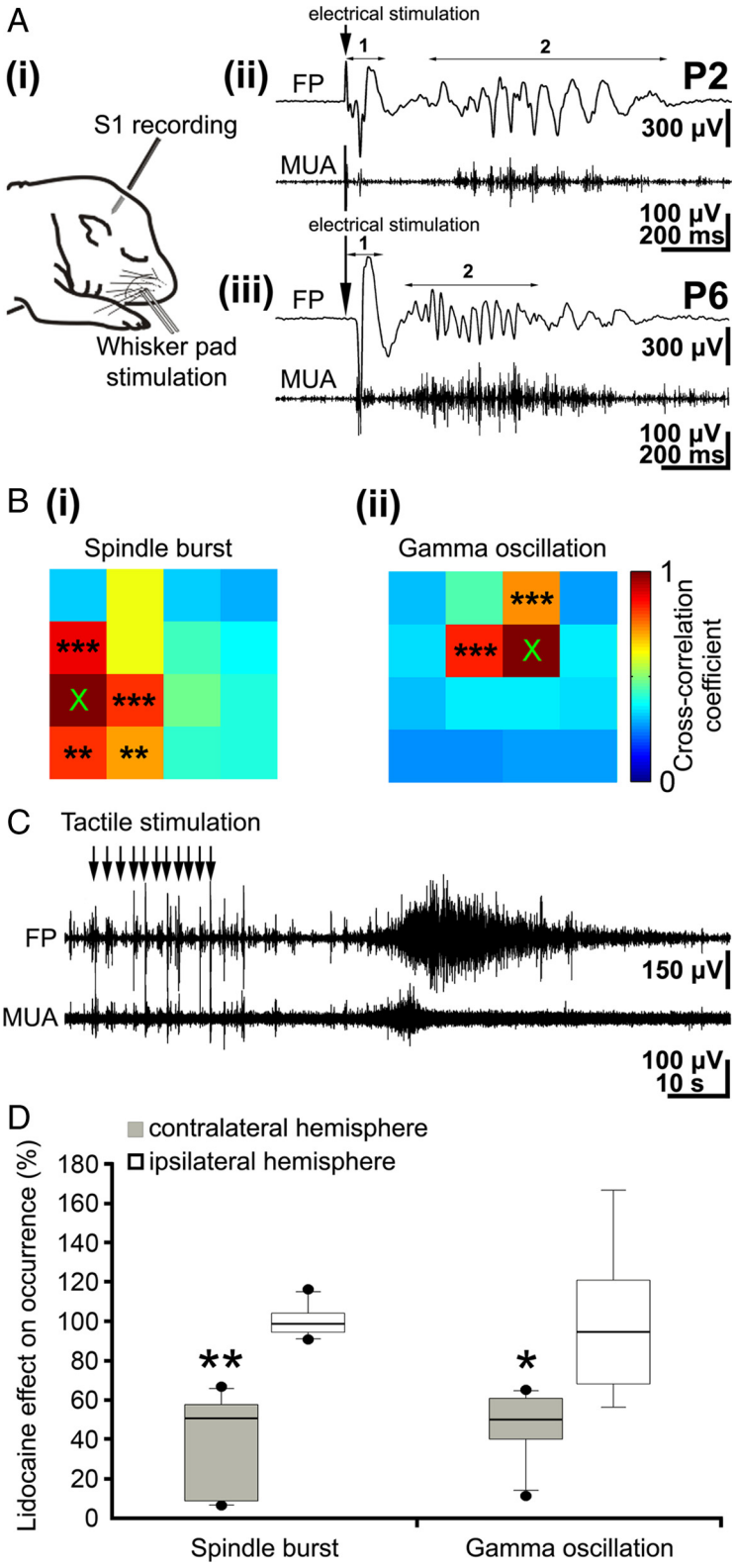

Figure 9. Stimulation of the periphery evokes neocortical oscillatory activity patterns. ***A***, ***i***, Scheme of experimental paradigm allowing electrical stimulation of the whisker pad and simultaneous recording of the field potential and MUA in the contralateral barrel cortex. ***ii***, Field potential (top) and MUA (below) recordings of the contralateral S1 response to a single electrical stimulus of the whisker pad in a P2 rat. The robust direct response (1) is followed by a spindle burst (2) correlated with prominent MUA. ***iii***, Field potential (top) and MUA (below) recordings of the contralateral S1 cortical response to electrical stimulation of the whisker pad in a P6 rat. The direct response (1) is followed by a gamma oscillation (2) correlated with MUA. ***B***, Color-coded plot of maximal cross-correlation coefficients calculated for spindle bursts (***i***) and gamma oscillations (***ii***) elicited by electrical stimulation of the whisker pad. Asterisks indicate significant cross-correlation coefficients compared with the reference channel marked by ×. ***C***, Field potential (top) and MUA (below) recordings of the contralateral S1 cortical response to repetitive tactile stimulation of the whiskers (11 times at ~1 Hz) in a P6 rat. Repetitive stimulation of the sensory input elicits a robust long oscillation correlated with MUA. ***D***, Effects of transient peripheral deafferentation by injection of lidocaine into the whisker pad on spontaneous spindle bursts and gamma oscillations. Box plots display the relative occurrence of spindle bursts (left) and gamma oscillations (right) recorded in six pups in the contralateral (black bars) and ipsilateral (white bars) barrel cortex after lidocaine injection.

terns synchronize spatially and temporally distinct neuronal networks; (3) spatially confined synchronized activity may contribute to the refinement of function-related architecture of the developing barrel field; (4) the subplate, gap junctional coupling, and NMDA receptor-mediated synaptic transmission are involved in the generation of these early oscillatory activity patterns *in vivo*.

Spindle bursts

Spindle bursts of 1–2 s in duration and ~10 Hz in frequency occur approximately every 10 s. They have been observed previously in the somatosensory (Khazipov et al., 2004; Minlebaev et al., 2007) and visual (Hanganu et al., 2006) cortices and represent the dominant pattern of neocortical activity in the newborn rat *in vivo*. The proposed inhibitory role of gap junctions in the generation of spindle bursts (Minlebaev et al., 2007, 2009) is currently difficult to explain because gap junction blockers generally have a suppressive effect on neuronal activity. Spindle burst activity resembles in many aspects the so-called delta-brush oscillations recorded with EEG in preterm human neonates of 29–31 weeks of postconceptional age (Milh et al., 2007; Vecchierini et al., 2007) (for recent review of EEG activity in preterm and neonatal babies, see Vanhatalo and Kaila, 2006). Khazipov et al. (2004) demonstrated in newborn rat somatosensory cortex that spindle bursts are spatially confined and selectively triggered in a somatotopic manner by spontaneous movements via sensory feedback signals. Our results are not only in good agreement with these previous observations but document the specific contribution of this activity pattern in the synchronization of a column-like neocortical network. Similar local network oscillations have been observed previously in the *in vitro* preparation of the intact cerebral cortex of the newborn rodent after activation of muscarinic or metabotropic glutamate receptors (Dupont et al., 2006; Wagner and Luhmann, 2006). However, under these conditions and with bath application of selec-

tive agonists to trigger the network oscillations, the activity propagates over large cortical regions (Peinado, 2000; Kilb and Luhmann, 2003; Calderon et al., 2005). Direct activation of the cholinergic basal forebrain *in vivo* facilitated the generation of spindle bursts (Hanganu et al., 2007), but the activity did not propagate.

Beside intracortical network mechanisms and neuromodulatory subcortical inputs, the main trigger for spindle bursts in rodents as well as for delta brushes in human babies comes from the sensory periphery (Khazipov et al., 2004; Hanganu et al., 2006; Milh et al., 2007; Minlebaev et al., 2007). We demonstrate that electrical stimulation of the whisker pad as well as tactile activation of the whiskers elicited spatially confined spindle bursts in the contralateral barrel cortex. The spatial organization and precise synchronization of neonatal spindle bursts indicate that this early activity pattern may serve as a template for the development of cortical barrels. A small number of spindle bursts were synchronized between both hemispheres and the degree of synchronization increased significantly during the first postnatal week. This interhemispheric synchronization is most likely mediated by callosal connections, which are innervating the subplate as early as P0 (Ivy and Killackey, 1981). It has been demonstrated that early neuronal activity is necessary for the normal development and maintenance of these callosal projections (Wang et al., 2007) and that the corpus callosum may modulate functionally inhibitory interactions between homotopic regions of the newborn rodent somatosensory cortex (Marcano-Reik and Blumberg, 2008).

Gamma oscillations

Gamma oscillations have been demonstrated previously in the newborn rat hippocampus *in vitro* (Palva et al., 2000) and with EEG techniques in the cerebral cortex of 8-month-old infants (Csibra et al., 2000). Here we describe *in vivo* gamma oscillations in the cerebral cortex of the newborn rodent, which in ontogenetic comparison resembles the prenatal state of the human cerebral cortex (Romijn et al., 1991). Gamma oscillations in the newborn rat somatosensory cortex revealed a frequency of 30–40 Hz, duration of 150–300 ms, and occurred every 10–30 s. Spontaneous as well as evoked spatially confined gamma oscillations were restricted to the barrel field, demonstrating the existence of a functional whisker representations at a time when the thalamocortical projection to layer IV itself is not even present. Because in rodents the subplate is already innervated by the thalamic input at late embryonic stages (Schlaggar and O'Leary, 1994; Higashi et al., 2002; Molnár et al., 2003), this periphery-driven gamma activity can be transferred to the developing cortex only via the subplate. We have suggested previously that the subplate does not only operate as a transient passive relay station between the thalamus and the developing cerebral cortex but rather as an active element amplifying the incoming neuronal activity and converting it into local synchronized oscillations (Dupont et al., 2006). Here we show that the subplate is involved in the generation of oscillatory activity *in vivo*.

Propagating long oscillations

Whereas spontaneous and stimulus-evoked spindle bursts and gamma oscillations did not propagate and both patterns synchronized a local neuronal network, the long oscillations propagated over large cortical regions and synchronized in the 10–20 Hz frequency range the activity over 600–800 μm. An activity pattern lasting up to 83 s have been recorded previously with EEG in premature infants from 24 to 27 weeks of gestation (Vecchierini et al., 2007). From all activity patterns observed in the newborn rat cerebral cortex, the long oscillations revealed the largest amplitude (250–750 μV) and longest duration (>40 s). However, this activity pattern occurred only every ~20 min. In a previous report, we describe a similar spontaneous oscillatory pattern with a faster propagation velocity in newborn mouse somatosensory cortical slices *in vitro* (Sun and Luhmann, 2007, their Fig. 2). Moreover, long-lasting propagating activity has been described as prominent calcium wave activity in the neonatal mouse cortex *in vivo* (Adelsberger et al., 2005). We have shown recently that transient activation of muscarinic receptors on subplate neurons elicits a long-lasting oscillatory activity in the newborn rat somatosensory cortex (Hanganu et al., 2009). This large-scale propagating activity pattern may interact with the nonpropagating local spindle bursts and gamma oscillations in an activity-depending manner, thereby promoting the formation of early neuronal ensembles. Interestingly subplate neurons show a pronounced facilitation during intracortical stimulation in the 10–40 Hz frequency range (Hirsch and Luhmann, 2008). Propagating long oscillations activate the developing cortex, including the subplate in this frequency range and may boost the periphery-driven input.

Physiological and pathophysiological relevance

The topographic development of the thalamocortical connections and the maturation of cortical columns depends on guidance molecules and electrical activity (López-Bendito and Molnár, 2003; Price et al., 2006). An increasing number of experimental evidence indicates that both processes interact and that transcription factors and patterned neuronal activity are both important for the formation of early connections and local neuronal networks (Hanson and Landmesser, 2004; Torborg et al., 2005; Dunn et al., 2006; Pfeiffenberger et al., 2006; Nicol et al., 2007). Not only spontaneous neuronal activity (Huberman et al., 2006) but, at a later developmental stage, also sensory activity are required for the formation and remodeling of topographic connections (Hooks and Chen, 2006). Our report characterizes in detail the spontaneous and evoked activity patterns of the newborn rat S1 *in vivo* and demonstrates the columnar-like organization and precise synchronization of these early activity patterns. Spindle bursts synchronize a neuronal network of 200–400 μm in diameter, and gamma oscillations are spatially confined to ~200 μm in the barrel field. These spatial dimensions correlate well with the diameter of a barrel in the somatosensory cortex of a neonatal rat (Schlaggar and O'Leary, 1994). Our data suggest that functional barrel-related columns already exist at the day of birth. Waters et al. (1990) suggested that an intrinsic template for the organization of cortical patterns may already exist during late embryonic development. If the thalamocortical input influences the cortical patterning at that early developmental stage, the subplate as a transient recipient zone for thalamocortical afferents must play an important role in this process (Allendoerfer and Shatz, 1994; Kostovic and Judas, 2002). Local electrical stimulation of the subplate *in vitro* elicits a gap junction-mediated oscillatory activity that synchronizes a columnar network of 100–150 μm in diameter (Dupont et al., 2006). The sensitivity of spindle bursts and gamma oscillations to carbenoxolone supports the role of gap junctional coupling for the generation of oscillatory activity *in vivo*. Additionally, the MUA and CSD profiles reinforce the role of the subplate in the generation of early activity patterns. The subplate may act as an amplifier that transmits the oscillatory activity to the overlying cortical plate (Hanganu et al., 2009). In the subplate and developing cortical plate, neurons are coupled via gap junctions and form early functional columnar networks (Yuste et al., 1992). This early columnar arrangement may originate from the gap junctional coupling between radial glial cells and migrating neurons (Elias et al.,

2007; Elias and Kriegstein, 2008), as initially suggested by Rakic (1988) in the "radial unit hypothesis."

Disturbances of neuronal network activity during early ontogenesis may interfere with developmental programs and may cause long-term alterations in cortical microcircuitry (Penn and Shatz, 1999; Le Van Quyen et al., 2006). The formation of cortical columns may be disturbed, leading to cognitive dysfunction (Levitt et al., 2004). Because the subplate plays a central role in early cortical development, structural and/or functional changes in the subplate and disturbances of early cortical activity patterns have been correlated with certain neurological deficits, such as epilepsy, schizophrenia, or autism (Bunney et al., 1997; Bunney and Bunney, 2000; McQuillen and Ferriero, 2005; Le Van Quyen et al., 2006). Experimental and clinical evidence indicate that EEG measurements in preterm infants may be of central importance to monitor cortical activity and to detect pathophysiological alterations at earliest developmental stages (Vanhatalo and Kaila, 2006).

References

Adelsberger H, Garaschuk O, Konnerth A (2005) Cortical calcium waves in resting newborn mice. Nat Neurosci 8:988–990.

Allendoerfer KL, Shatz CJ (1994) The subplate, a transient neocortical structure: its role in the development of connections between thalamus and cortex. Annu Rev Neurosci 17:185–218.

Ben-Ari Y, Gaiarsa JL, Tyzio R, Khazipov R (2007) GABA: a pioneer transmitter that excites immature neurons and generates primitive oscillations. Physiol Rev 87:1215–1284.

Bunney BG, Potkin SG, Bunney WE (1997) Neuropathological studies of brain tissue in schizophrenia. J Psychiatr Res 31:159–173.

Bunney WE, Bunney BG (2000) Evidence for a compromised dorsolateral prefrontal cortical parallel circuit in schizophrenia. Brain Res Rev 31:138–146.

Calderon DP, Leverkova N, Peinado A (2005) $G_{q/11}$-induced and spontaneous waves of coordinated network activation in developing frontal cortex. J Neurosci 25:1737–1749.

Cang J, Rentería RC, Kaneko M, Liu X, Copenhagen DR, Stryker MP (2005) Development of precise maps in visual cortex requires patterned spontaneous activity in the retina. Neuron 48:797–809.

Crépel V, Aronov D, Jorquera I, Represa A, Ben-Ari Y, Cossart R (2007) A parturition-associated nonsynaptic coherent activity pattern in the developing hippocampus. Neuron 54:105–120.

Csibra G, Davis G, Spratling MW, Johnson MH (2000) Gamma oscillations and object processing in the infant brain. Science 290:1582–1585.

Demas J, Sagdullaev BT, Green E, Jaubert-Miazza L, McCall MA, Gregg RG, Wong RO, Guido W (2006) Failure to maintain eye-specific segregation in nob, a mutant with abnormally patterned retinal activity. Neuron 50:247–259.

Dunn TA, Wang CT, Colicos MA, Zaccolo M, DiPilato LM, Zhang J, Tsien RY, Feller MB (2006) Imaging of cAMP levels and protein kinase A activity reveals that retinal waves drive oscillations in second-messenger cascades. J Neurosci 26:12807–12815.

Dupont E, Hanganu IL, Kilb W, Hirsch S, Luhmann HJ (2006) Rapid developmental switch in the mechanisms driving early cortical columnar networks. Nature 439:79–83.

Elias LA, Kriegstein AR (2008) Gap junctions: multifaceted regulators of embryonic cortical development. Trends Neurosci 31:243–250.

Elias LA, Wang DD, Kriegstein AR (2007) Gap junction adhesion is necessary for radial migration in the neocortex. Nature 448:901–907.

Feller MB, Scanziani M (2005) A precritical period for plasticity in visual cortex. Curr Opin Neurobiol 15:94–100.

Galli L, Maffei L (1988) Spontaneous impulse activity of rat retinal ganglion cells in prenatal life. Science 242:90–91.

Garaschuk O, Linn J, Eilers J, Konnerth A (2000) Large-scale oscillatory calcium waves in the immature cortex. Nat Neurosci 3:452–459.

Hanganu IL, Ben-Ari Y, Khazipov R (2006) Retinal waves trigger spindle bursts in the neonatal rat visual cortex. J Neurosci 26:6728–6736.

Hanganu IL, Staiger JF, Ben-Ari Y, Khazipov R (2007) Cholinergic modulation of spindle bursts in the neonatal rat visual cortex *in vivo*. J Neurosci 27:5694–5705.

Hanganu IL, Okabe A, Lessmann V, Luhmann HJ (2009) Cellular mechanisms of subplate-driven and cholinergic input-dependent network activity in the neonatal rat somatosensory cortex. Cereb Cortex 19:89–105.

Hanson MG, Landmesser LT (2003) Characterization of the circuits that generate spontaneous episodes of activity in the early embryonic mouse spinal cord. J Neurosci 23:587–600.

Hanson MG, Landmesser LT (2004) Normal patterns of spontaneous activity are required for correct motor axon guidance and the expression of specific guidance molecules. Neuron 43:687–701.

Higashi S, Molnár Z, Kurotani T, Toyama K (2002) Prenatal development of neural excitation in rat thalamocortical projections studied by optical recording. Neuroscience 115:1231–1246.

Hirsch S, Luhmann HJ (2008) Pathway-specificity in *N*-methyl-D-aspartate receptor-mediated synaptic inputs onto subplate neurons. Neuroscience 153:1092–1102.

Hooks BM, Chen C (2006) Distinct roles for spontaneous and visual activity in remodeling of the retinogeniculate synapse. Neuron 52:281–291.

Huberman AD, Speer CM, Chapman B (2006) Spontaneous retinal activity mediates development of ocular dominance columns and binocular receptive fields in v1. Neuron 52:247–254.

Ivy GO, Killackey HP (1981) The ontogeny of the distribution of callosal projection neurons in the rat parietal cortex. J Comp Neurol 195:367–389.

Jerbi K, Lachaux JP, N'Diaye K, Pantazis D, Leahy RM, Garnero L, Baillet S (2007) Coherent neural representation of hand speed in humans revealed by MEG imaging. Proc Natl Acad Sci U S A 104:7676–7681.

Khazipov R, Luhmann HJ (2006) Early patterns of electrical activity in the developing cerebral cortex of human and rodents. Trends Neurosci 29:414–418.

Khazipov R, Sirota A, Leinekugel X, Holmes GL, Ben-Ari Y, Buzsáki G (2004) Early motor activity drives spindle bursts in the developing somatosensory cortex. Nature 432:758–761.

Kilb W, Luhmann HJ (2003) Carbachol-induced network oscillations in the intact cerebral cortex of the newborn rat. Cereb Cortex 13:409–421.

Kostovic I, Judas M (2002) The role of the subplate zone in the structural plasticity of the developing human cerebral cortex. Neuroembryology 1:145–153.

Krupa DJ, Ghazanfar AA, Nicolelis MA (1999) Immediate thalamic sensory plasticity depends on corticothalamic feedback. Proc Natl Acad Sci U S A 96:8200–8205.

Lahtinen H, Palva JM, Sumanen S, Voipio J, Kaila K, Taira T (2002) Postnatal development of rat hippocampal gamma rhythm in vivo. J Neurophysiol 88:1469–1474.

Leinekugel X, Khazipov R, Cannon R, Hirase H, Ben-Ari Y, Buzsáki G (2002) Correlated bursts of activity in the neonatal hippocampus in vivo. Science 296:2049–2052.

Le Van Quyen M, Khalilov I, Ben-Ari Y (2006) The dark side of high-frequency oscillations in the developing brain. Trends Neurosci 29:419–427.

Levitt P, Eagleson KL, Powell EM (2004) Regulation of neocortical interneuron development and the implications for neurodevelopmental disorders. Trends Neurosci 27:400–406.

López-Bendito G, Molnár Z (2003) Thalamocortical development: how are we going to get there? Nat Rev Neurosci 4:276–289.

Lu H, Hartmann MJ, Bower JM (2005) Correlations between Purkinje cell single-unit activity and simultaneously recorded field potentials in the immediately underlying granule cell layer. J Neurophysiol 94:1849–1860.

Marcano-Reik AJ, Blumberg MS (2008) The corpus callosum modulates spindle-burst activity within homotopic regions of somatosensory cortex in newborn rats. Eur J Neurosci 28:1457–1466.

McQuillen PS, Ferriero DM (2005) Perinatal subplate neuron injury: implications for cortical development and plasticity. Brain Pathol 15:250–260.

Meister M, Wong RO, Baylor DA, Shatz CJ (1991) Synchronous bursts of action potentials in ganglion cells of the developing mammalian retina. Science 252:939–943.

Milh M, Kaminska A, Huon C, Lapillonne A, Ben-Ari Y, Khazipov R (2007) Rapid cortical oscillations and early motor activity in premature human neonate. Cereb Cortex 17:1582–1594.

Minlebaev M, Ben-Ari Y, Khazipov R (2007) Network mechanisms of spindle-burst oscillations in the neonatal rat barrel cortex in vivo. J Neurophysiol 97:692–700.

Minlebaev M, Ben-Ari Y, Khazipov R (2009) NMDA receptors pattern early activity in the developing barrel cortex in vivo. Cereb Cortex 19:688–696.

Molnár Z, Adams R, Blakemore C (1998) Mechanisms underlying the early establishment of thalamocortical connections in the rat. J Neurosci 18:5723–5745.

Molnár Z, Kurotani T, Higashi S, Yamamoto N, Toyama K (2003) Development of functional thalamocortical synapses studied with current

source-density analysis in whole forebrain slices in the rat. Brain Res Bull 60:355–371.

Nicholson C, Freeman JA (1975) Theory of current source-density analysis and determination of conductivity tensor for anuran cerebellum. J Neurophysiol 38:356–368.

Nicol X, Voyatzis S, Muzerelle A, Narboux-Nême N, Südhof TC, Miles R, Gaspar P (2007) cAMP oscillations and retinal activity are permissive for ephrin signaling during the establishment of the retinotopic map. Nat Neurosci 10:340–347.

Palva JM, Lamsa K, Lauri SE, Rauvala H, Kaila K, Taira T (2000) Fast network oscillations in the newborn rat hippocampus *in vitro*. J Neurosci 20:1170–1178.

Paxinos G, Törk I, Tecott LH, Valentino KL (1991) Atlas of the developing rat brain. San Diego: Academic.

Peinado A (2000) Traveling slow waves of neural activity: a novel form of network activity in developing neocortex. J Neurosci 20:RC54(1–6).

Peinado A (2001) Immature neocortical neurons exist as extensive syncitial networks linked by dendrodendritic electrical connections. J Neurophysiol 85:620–629.

Penn AA, Shatz CJ (1999) Brain waves and brain wiring: the role of endogenous and sensory-driven neural activity in development. Pediatr Res 45:447–458.

Pfeiffenberger C, Yamada J, Feldheim DA (2006) Ephrin-As and patterned retinal activity act together in the development of topographic maps in the primary visual system. J Neurosci 26:12873–12884.

Price DJ, Kennedy H, Dehay C, Zhou L, Mercier M, Jossin Y, Goffinet AM, Tissir F, Blakey D, Molnár Z (2006) The development of cortical connections. Eur J Neurosci 23:910–920.

Rakic P (1988) Specification of cerebral cortical areas. Science 241:170–176.

Romijn HJ, Hofman MA, Gramsbergen A (1991) At what age is the developing cerebral cortex of the rat comparable to that of the full-term newborn human baby? Early Hum Dev 26:61–67.

Rousseeuw PJ (1987) Silhouettes: a graphical aid to the interpretation and validation of cluster-analysis. J Comput Appl Math 20:53–65.

Saint-Amant L, Drapeau P (2001) Synchronization of an embryonic network of identified spinal interneurons solely by electrical coupling. Neuron 31:1035–1046.

Schlaggar BL, O'Leary DDM (1994) Early development of the somatotopic map and barrel patterning in rat somatosensory cortex. J Comp Neurol 346:80–96.

Shaw FZ, Liao YF (2005) Relation between activities of the cortex and vibrissae muscles during high-voltage rhythmic spike discharges in rats. J Neurophysiol 93:2435–2448.

Sun JJ, Luhmann HJ (2007) Spatio-temporal dynamics of oscillatory network activity in the neonatal mouse cerebral cortex. Eur J Neurosci 26:1995–2004.

Torborg CL, Feller MB (2005) Spontaneous patterned retinal activity and the refinement of retinal projections. Prog Neurobiol 76:213–235.

Torborg CL, Hansen KA, Feller MB (2005) High frequency, synchronized bursting drives eye-specific segregation of retinogeniculate projections. Nat Neurosci 8:72–78.

Vanhatalo S, Kaila K (2006) Development of neonatal EEG activity: from phenomenology to physiology. Semin Fetal Neonatal Med 11:471–478.

Vecchierini MF, André M, d'Allest AM (2007) Normal EEG of premature infants born between 24 and 30 weeks gestational age: terminology, definitions and maturation aspects. Neurophysiol Clin 37:311–323.

Wagner J, Luhmann HJ (2006) Activation of metabotropic glutamate receptors induces propagating network oscillations in the intact cerebral cortex of the newborn mouse. Neuropharmacology 51:848–857.

Wang CL, Zhang L, Zhou Y, Zhou J, Yang XJ, Duan SM, Xiong ZQ, Ding YQ (2007) Activity-dependent development of callosal projections in the somatosensory cortex. J Neurosci 27:11334–11342.

Waters RS, McCandlish CA, Cooper NG (1990) Early development of SI cortical barrel subfield representation of forelimb in normal and deafferented neonatal rat as delineated by peroxidase conjugated lectin, peanut agglutinin (PNA). Exp Brain Res 81:234–240.

Welker C (1976) Receptive fields of barrels in the somatosensory neocortex of the rat. J Comp Neurol 166:173–189.

Yuste R, Peinado A, Katz LC (1992) Neuronal domains in developing neocortex. Science 257:665–669.

Yuste R, Nelson DA, Rubin WW, Katz LC (1995) Neuronal domains in developing neocortex: mechanisms of coactivation. Neuron 14:7–17.